

AD-A280 187



1

Carderock Division, Naval Surface Warfare Center

Bethesda, Maryland 20084-5000

CARDIVNSWC-94/003

April 1994

Ship Systems and Programs Directorate
Research and Development Report

Marangoni Convection in a Gravity-Free Silicon Float Zone

by
Samuel Ohring
Hans J. Lugt

Marangoni Convection in a Gravity-Free Silicon Float Zone

DTIC
ELECTE
JUN 10 1994
S G D

94-17777



5280



Approved for public release; distribution is unlimited.

CARDIVNSWC-94/003

94 6 9 090

REPORT DOCUMENTATION PAGE

1a. REPORT SECURITY CLASSIFICATION UNCLASSIFIED		1b. RESTRICTIVE MARKINGS	
2a. SECURITY CLASSIFICATION AUTHORITY See reverse side.		3 DISTRIBUTION/AVAILABILITY OF REPORT Approved for public release; distribution is unlimited.	
2b. DECLASSIFICATION/DOWNGRADING SCHEDULE			
4. PERFORMING ORGANIZATION REPORT NUMBER(S) CARDIVNSWC-94/003		5. MONITORING ORGANIZATION REPORT NUMBER(S)	
6a. NAME OF PERFORMING ORGANIZATION Carderock Division Naval Surface Warfare Center	6b. OFFICE SYMBOL (If applicable) Code 2041	7a. NAME OF MONITORING ORGANIZATION	
6c. ADDRESS (City, State, and ZIP Code) Bethesda, MD 20084-5000		7b. ADDRESS (CITY, STATE, AND ZIP CODE)	
8a. NAME OF FUNDING/SPONSORING ORGANIZATION NASA Lewis Research Center	8b. OFFICE SYMBOL (If applicable)	9. PROCUREMENT INSTRUMENT IDENTIFICATION NUMBER	
8c. ADDRESS (City, State, and ZIP code) Cleveland, Ohio 44135		10. SOURCE OF FUNDING NUMBERS	
		PROGRAM ELEMENT NO.	PROJECT NO. C-32007-14
		TASK NO.	WORK UNIT ACCESSION NO. DN 509316
11. TITLE (Include Security Classification) Marangoni Convection in a Gravity-Free Silicon Float Zone			
12. PERSONAL AUTHOR(S) Lugt, Hans J., and Ohring, Samuel			
13a. TYPE OF REPORT Final	13b. TIME COVERED FROM _____ TO _____	14. DATE OF REPORT (Year, Month, Day) 1994 April	15. PAGE COUNT 53
16. SUPPLEMENTARY NOTATION			
17. COSATI CODES		18. SUBJECT TERMS (Continue on Reverse if Necessary and Identify by Block Number)	
FIELD	GROUP	SUB-GROUP	
19. ABSTRACT (Continue on reverse if necessary and identify by block number) The onset of Marangoni convection in the float zone of liquid silicon is studied from a state at rest in the absence of gravity. This time-dependent flow problem is solved numerically with the aid of the Navier-Stokes equations for an axisymmetric flow with nonlinear free surface conditions. On this free surface the temperature gradient is generated by heat transfer and radiation from a heater, which is symmetrically located between the two walls of the float zone. After a certain time, the flow is asymmetrically disturbed by moving the heater for a short time away from its symmetric position and back. Three different Marangoni numbers (based on the temperature difference between heater and melting point of silicon) are computed: 10,400, 30,225, and 50,050. The results show that for $Ma = 10,400$ the flow is steady and stable. For the two higher Marangoni numbers, however, the disturbed flows become unstable, and persistent oscillatory modes of 0.22 Hz for $Ma = 30,225$ and 0.27 Hz for $Ma = 50,050$ develop. (Continued on reverse side.)			
20. DISTRIBUTION/AVAILABILITY OF ABSTRACT <input checked="" type="checkbox"/> UNCLASSIFIED/UNLIMITED <input type="checkbox"/> SAME AS RPT. <input type="checkbox"/> DTIC USERS		21. ABSTRACT SECURITY CLASSIFICATION UNCLASSIFIED	
22a. NAME OF RESPONSIBLE INDIVIDUAL Hans J. Lugt		22b. TELEPHONE (Include Area Code) (301) 227-1925	22c. OFFICE SYMBOL Code 2040.1

UNCLASSIFIED

SECURITY CLASSIFICATION OF THIS PAGE

Block 19. Abstract (Continued)

The free surface itself is little deformed but computation with a flat surface confirms Kazarinoff and Wilkowski's 1989 result that the flat surface suppresses instability. It is conjectured that the flat surface imposes a strong local flow symmetry, which has a damping effect, and that, in the case of a deformable free surface, instability and maintenance of oscillation occur when the two rolls attached to the corners, which are formed by the wall and the free surface, separate and become vortices with extremal vorticity. These two vortices interact rhythmically by alternating build-up and decay.

Accession For	
NTIS CRA&I	<input checked="checked" type="checkbox"/>
DTIC TAB	<input type="checkbox"/>
Unannounced	<input type="checkbox"/>
Justification	
By	
Distribution /	
Availability Codes	
Dist	Avail and/or Special
A-1	

CONTENTS

	Page
ABSTRACT	1
ADMINISTRATIVE INFORMATION	1
INTRODUCTION	1
THE INITIAL-BOUNDARY VALUE PROBLEM	3
OUTLINE OF THE NUMERICAL PROCEDURE	6
RESULTS	8
CONCLUSIONS	13
ACKNOWLEDGMENTS	14
REFERENCES	14

FIGURES

1. Sketch of a float zone with streamlines and ring heater after Schwabe et al. (1978)	16
2. Model of the float zone with temperature distribution of the ring heater	16
3. Numerical grid layout	17
4. Lines of constant ω_ϕ/r for $Ma = 10,400$ at six different times	18
5. Close-up of lines of constant ω_ϕ/r for $Ma = 10,400$ in the core region of Fig. 4, $t = 10.5s$	19
6. Equivorticity lines (lines of constant ω_ϕ) for $Ma = 10,400$ at $t = 10.5s$	20
7. Surface vorticity (= negative surface shear stress) for $Ma = 10,400$ of the vorticity field in Fig. 4	21
8. Streamlines of the vorticity field in Fig. 4 at three different times	22
9. Isotherms for $Ma = 10,400$ at six different times	23
10. Surface temperature for $Ma = 10,400$ of the temperature field in Fig. 9	24
11. Surface vorticity for $Ma = 10,400$ at $z = 0$ as a function of time	25
12. Surface velocity w_r for $Ma = 10,400$ at $t = 10.5s$	26

13. Lines of constant ω_ϕ/r for $Ma = 50,050$ at four different times before and after the asymmetric disturbance	27
14. Lines of constant ω_ϕ/r in the core regions of Fig. 13	28
15. Surface vorticity for $Ma = 50,050$ of the vorticity field in Fig. 13	29
16. Streamlines for $Ma = 50,050$ at two different times	31
17. Surface vorticity for $Ma = 50,050$ at $z' = 0.5$ cm and at $z' = 0.0125$ cm as a function of time	32
18. Isotherms for $Ma = 50,050$ at the times $t = 1.5, 1.72, 2.5, 4.0s$	33
19. Surface temperature for $Ma = 50,050$ of the temperature field in Fig. 18	34
20. Lines of constant ω_ϕ/r of a $5/4$ cycle computed for $Ma = 50,050$ at six different times	35
21. Lines of constant ω_ϕ/r in the core region of the rolls depicted in Fig. 20	36
22. Equivorticity lines for $Ma = 50,050$ in the right core region at $t = 27, 28, 29, 30s$	38
23. Surface vorticity for $Ma = 50,050$ of the vorticity field in Fig. 20 at three different times	39
24. Surface velocity for $Ma = 50,050$ of the vorticity field in Fig. 20 at three different times	40
25. Streamlines for $Ma = 50,050$ of the vorticity field in Fig. 20 at four different times	41
26. Isotherms for $Ma = 50,050$ corresponding to the flow field in Fig. 25	42
27. Surface temperature for $Ma = 50,050$ at six different times in a computed cycle	43
28. $\partial T/\partial z$ along the left wall as a measure for the heat flux into the wall	44
29. Close-up of lines of constant ω_ϕ/r for $Ma = 50,050$ near the surface location of $(\omega_\phi)_s = 0$ at $t = 27, 28, 29s$	45
30. Surface vorticity on a flat free surface for $Ma = 50,050$ at $z' = 0.5$ cm and at $z' = 0.0125$ cm as a function of time after the change in the surface conditions at $t = 26s$	46

Table 1. List of constants for silicon	5
--	---

ABSTRACT

The onset of Marangoni convection in the float zone of liquid silicon is studied from a state at rest in the absence of gravity. This time-dependent flow problem is solved numerically with the aid of the Navier-Stokes equations for an axisymmetric flow with nonlinear free surface conditions. On this free surface the temperature gradient is generated by heat transfer and radiation from a heater, which is symmetrically located between the two walls of the float zone. After a certain time, the flow is asymmetrically disturbed by moving the heater for a short time away from its symmetric position and back. Three different Marangoni numbers (based on the temperature difference between heater and melting point of silicon) are computed: 10,400, 30,225, and 50,050. The results show that for $Ma = 10,400$ the flow is steady and stable. For the two higher Marangoni numbers, however, the disturbed flows become unstable, and persistent oscillatory modes of 0.22 Hz for $Ma = 30,225$ and 0.27 Hz for $Ma = 50,050$ develop. The free surface itself is little deformed but computation with a flat surface confirms Kazarinoff and Wilkowski's 1989 result that the flat surface suppresses instability. It is conjectured that the flat surface imposes a strong local flow symmetry, which has a damping effect, and that, in the case of a deformable free surface, instability and maintenance of oscillation occur when the two rolls attached to the corners, which are formed by the wall and the free surface, separate and become vortices with extremal vorticity. These two vortices interact rhythmically by alternating build-up and decay.

ADMINISTRATIVE INFORMATION

This work was supported by the NASA-Microgravity Program under Order No. C-32007-M of the NASA Lewis Research Center.

INTRODUCTION

In outer space the growth of silicon crystals with high purity can be achieved in a greatly reduced gravity field, so that the melt is not disturbed by fluid motion due to buoyancy. Containerless devices, which are proposed to avoid chemical reactions between melt and container, have interfaces between melt and an inert-gas environment. However, the temperature gradient between heater and solid silicon, when the heat is transmitted across and along the interface, causes a gradient of the surface tension that generates a fluid flow in the melt. This surface-tension driven flow is called *Marangoni convection* or *thermocapillary convection* and can occur in steady and unsteady (non-oscillatory or oscillatory) modes that are separated by a critical flow parameter.¹⁻² The latter unsteady flow is particularly undesirable for crystal growing because an unsteady flow affects the quality of silicon chips considerably. Methods such as rotating the float zone,³ MHD effects,⁴ and counteracting jets⁵ have been proposed to suppress this undesired fluid motion.

The numerical study of Marangoni convection in microgravity has been covered extensively in the literature for a number of devices with various degrees of model sophistication. Review papers and recent publications with background references include those by Ostrach,⁶ Linde,⁷ Preisser *et al.*,⁸ Schwabe,⁹ Young and Chait,¹⁰ and the GAMM

Workshop, Roux.¹¹ (The GAMM Workshop dealt essentially with a "benchmark" model which is different from this paper's approach).

This paper is based on the arrangement, sketched in Fig. 1. Liquid silicon is held together between two coaxial circular-cylindrical rods of solid silicon by the surface tension of the liquid-gas interface in a microgravity environment. The liquid bridge between the two rods is called the *float zone*. The heat for the melting process is provided by a ring heater which moves coaxially over the rod. During that time solid silicon is molten and then freezes to a monocrystal. This process is modeled according to Fig. 2 with the following simplifications: The boundaries between molten and solid silicon are considered planar with melting and freezing neglected. On the liquid-gas interface, the effect of the gas on the liquid shear stress is neglected, that is, the interface is considered a "free surface." The flow region is assumed axisymmetric and, together with the ring heater, fixed. However, no symmetry along the center plane between the two walls is enforced so that an oscillatory flow over the whole float zone can be studied. At the time $t = 0$ the liquid silicon has the melting temperature $T = T_M$, and at this instant, the heater is turned on to a maximum temperature $T_H > T_M$. The developing temperature gradient along the free surface creates the stress for the Marangoni flow which in time penetrates into the interior of the float zone. For small differences in the temperatures T_H and T_M a steady state will be reached after a certain time. Beyond a critical difference $T_H - T_M$ the flow is expected to become unstable, and a time-dependent mode (non-oscillatory or oscillatory) in the direction parallel to the axis might appear. It is the purpose of this paper to find these two modes and to analyze the corresponding flow and temperature fields.

The source of energy, which drives the Marangoni convection, comes from the ring heater and is transmitted through the free surface. In mathematical terms, a temperature gradient (perpendicular to the surface) is generated by heat radiation and heat transfer from the ring heater. The boundary conditions on the free surface and the geometric representation of the adjacent immediate flow region are hence very sensitive to both physical and numerical modeling. It was found by Kamotani *et al.*¹² and by Kazarinoff and Wilkowski¹³ that the nonlinear free surface conditions should not be linearized (that is, a flat surface should not be assumed) as most other researchers have done because surface deformation would initiate instability from a critical $T_H - T_M$ on. To check their finding, the full nonlinear free-surface conditions are retained in this paper. It may be mentioned that experiments¹⁴ indicate only a slight deviation of the real surface from the flat cylindrical one, a fact which might not, however, exclude a sensitivity of the deformable free surface toward flow instability (a fact confirmed in this paper).

The most serious restrictions of this flow model are axisymmetry and planar end walls of the rods, with melting and freezing processes neglected. To a lesser degree the assumption of a fixed ring heater affects the study of the real float zone. The axisymmetry imposed on the flow prevents a full investigation of instability because the analysis of the various modes of instability is restricted to that of axisymmetric disturbances. Experiments with earth gravity for a much larger Prandtl number than that of liquid silicon have shown that azimuthal disturbances are more "dangerous" than axial ones.¹⁵ An argument for the importance of axisymmetric modes was given by Kazarinoff and Wilkowski.¹⁶ The definitive answer to the question of whether axisymmetric modes are crucial must be obtained from future studies.

Planar end walls of the rods can cause a singularity at the triple point of the solid, liquid, and gaseous phases. This singularity was mentioned by Zebib *et al.*¹⁷ In reality, as it

is conjectured from Fig. 1, a cusp might develop which prevents such a singularity. Here, the singularity cannot be avoided unless the assumption of a planar end wall is abandoned. Most researchers ignore this singularity because it appears to have only a local effect.

Liquid silicon has a Prandtl number of 0.023. There are only a few papers which deal with such a low Prandtl number. Non-axisymmetric oscillations of the float zone have been observed experimentally for high Prandtl-number flows by Kamotani *et al.*¹² who also argue that the deformable free surface is essential for the onset of instability. Kazarinoff and Wilkowski¹³ found numerically axisymmetric oscillations in a liquid-silicon float zone and Fowles and Roberts¹⁸ computed axisymmetric oscillations in a *rotating* liquid-silicon float zone. In a numerical study with a general three-dimensional flow code, Rupp *et al.*¹⁹ found azimuthal periodicity. However, their results are restricted to a half-zone, that is, they considered only the region $-L/2 \leq z \leq 0$ with a solid wall at $z = 0$ in Fig. 2 and an adiabatic free surface. The restriction to a half-zone applies also to recent instability studies.^{20,21} The only study, the authors are aware of, that was made with almost the same flow model but with a different numerical scheme and with a much coarser grid and time step, is recorded in a letter by Kazarinoff and Wilkowski.¹³ Unfortunately, there is not enough information to make a comparison with the present results, and an investigation of the discrepancies is not possible.

THE INITIAL-BOUNDARY VALUE PROBLEM

The mathematical description of the flow model is based on the Navier-Stokes equations for an incompressible Newtonian fluid. With cylindrical polar coordinates r, ϕ, z and the corresponding velocity components u, v, w , with axisymmetry $\partial/\partial\phi \equiv 0$, and $v \equiv 0$, the equations of motion and the energy equation are:

$$u_r + \frac{u}{r} + w_z = 0, \quad (1)$$

$$u_t + \frac{1}{r}(ru^2)_r + (uw)_z = -\frac{1}{\rho}p_r + \nu[u_{rr} + (\frac{u}{r})_r + u_{zz}], \quad (2)$$

$$w_t + \frac{1}{r}(ruw)_r + (w^2)_z = -\frac{1}{\rho}p_z + \nu[w_{rr} + \frac{1}{r}w_r + w_{zz}], \quad (3)$$

$$T_t + uT_r + wT_z = K[T_{rr} + \frac{1}{r}T_r + T_{zz}]. \quad (4)$$

Here, p, ρ, ν , and K are the pressure, the density, the kinematic viscosity, and the thermal diffusivity of the liquid silicon, respectively. It may be noticed that the conservation form of the nonlinear terms in Eqs. (2) and (3) is not retained in Eq. (4) for numerical reasons.

The boundary conditions for the float zone are (Fig. 2):

Cold surfaces:

$$z = \pm \frac{L}{2}, \quad 0 \leq r \leq R: \quad u = w = p_z = 0, \quad T = T_M. \quad (5)$$

Axis:

$$-\frac{L}{2} \leq z \leq +\frac{L}{2}, \quad r = 0: \quad u = 0, \quad w_r = p_r = T_r = 0. \quad (6)$$

The free surface is described by $r = h(z, t)$, and the boundary conditions are^{10,22}:

$$h_t = u - wh_z, \quad (7)$$

$$p - 2\mu u_r + \mu(u_z + w_r)h_z = -\sigma_M\left(\frac{1}{R_1} + \frac{1}{R_2}\right) - \sigma_r \sqrt{1 + h_z^2}, \quad (8)$$

$$(p - 2\mu w_z)h_z + \mu(u_z + w_r) = -\sigma_M\left(\frac{1}{R_1} + \frac{1}{R_2}\right)h_z + \sigma_z \sqrt{1 + h_z^2}, \quad (9)$$

where Eqs. (8) and (9) are the stress components in the r - and z -directions. It is

$$\frac{1}{R_1} + \frac{1}{R_2} = \frac{1}{\sqrt{1 + h_z^2}} \left(-\frac{1}{h} + \frac{h_{zz}}{1 + h_z^2} \right), \quad (10)$$

$$\sigma = \sigma_M - \gamma(T - T_M). \quad (11)$$

The constant coefficient of the surface tension is σ_M , γ is the temperature coefficient of the surface tension σ , μ is the dynamic viscosity with $\mu = \rho\nu$, and $1/R_1$ and $1/R_2$ are the surface curvatures in the planes $z = \text{const}$ and $\phi = \text{const}$, respectively.

For a flat free surface with $h_z = 0$, Eq. (7) reduces to $u = 0$, and one obtains from Eqs. (8) and (9) for the shear stress at the free surface

$$\mu w_r = \sigma_z = -\gamma T_z. \quad (12)$$

The occurrence of a jump in w_r at $z = \pm L/2$ can be seen immediately since w_r is equal to zero along the wall but nonzero at the triple point when this point is approached from the free surface. w_r can also be interpreted as negative vorticity. Because of the assumptions of axisymmetry and $v \equiv 0$, only the ϕ -component of the vorticity vector, defined by $\omega_\phi = u_z - w_r$, is nonzero.

The temperature distribution of the free surface is prescribed by the temperature gradient generated by the heat conduction and radiation from the heater

$$-k \frac{T_r - h_z T_z}{\sqrt{1 + h_z^2}} = \alpha(T - \theta) + \epsilon(T^4 - \theta^4), \quad (13)$$

$$\theta = T_M + (T_H - T_M) \exp \left[\frac{z^2 \log a}{L^2/4} \right], \quad (14)$$

The constant k is the thermal conductivity, α the heat transfer coefficient, s the Stefan-Boltzmann constant, ϵ the emissivity, and a is a distribution parameter of the heater function θ which approximates the heater. T_H refers to the maximum temperature of the heater.

Equation (4) imposes a feedback mechanism on the whole system in the form that, at each time step, Eq. (4) provides an update of the surface temperature which in turn affects the boundary conditions of the flow field. The update of the flow field then modifies the temperature field, and a new cycle starts. To improve the numerical stability the temperature field is computed with the known velocity field of the previous time step. The numerical error due to this procedure is extremely small. Thus, only one cycle between the temperature and velocity fields is necessary.

As initial conditions it is assumed that the fluid is at rest at the melting temperature T_M , that $p = \sigma_M$, that the free surface is flat ($h = R$), and that over an extremely short time span the temperature T_H of the heater is gradually turned on. In order to induce instability of the float zone, which so far is symmetric with respect to the plane $z = 0$, flow and temperature fields can be disturbed at a given instant by dislocating the ring heater for a certain time span. The initial-boundary value problem, defined by Eqs. (1) through (11), (13) and (14), can be made dimensionless in various ways. For instance, one could scale the velocity either by K/R or by $\gamma\Delta T/\mu$. In the latter case the following characteristic quantities would appear: length R , velocity $\gamma\Delta T/\mu$, time $R\mu/\gamma\Delta T$, temperature ΔT , and pressure $(\gamma\Delta T)^2/\mu\nu$. In addition to the Prandtl and Marangoni numbers (or Reynolds number $Re = Ma/Pr$), the Weber number $\gamma\Delta T/\sigma_M$ (which is here equal to the Capillary number), the Nusselt number $\alpha R/k$, and the radiation number $s\epsilon R\Delta T^3/k$ will occur. Since no simplifications (truncations) of the original boundary-value problem have been made, the dimensional form as well as the dimensionless models are equivalent. As in Refs. 13 and 16, because of the importance of silicon, the dimensional form is retained. The following data from Refs. 3 and 10 are used:

Table 1. List of constants for silicon.

$\rho = 2.5 \text{ g/cm}^3$
$\mu = 0.0088 \text{ g/cm s}$
$\nu = 0.0035 \text{ cm}^2/\text{s}$
$k = 0.32 \cdot 10^7 \text{ erg/cm s } ^\circ\text{C}$
$K = 0.15 \text{ cm}^2/\text{s}$
$\alpha = 0.64 \cdot 10^5 \text{ erg/s cm}^2 \text{ } ^\circ\text{C}$
$\sigma_M = 720 \text{ dyn/cm}$
$\gamma = 0.43 \text{ dyn/cm } ^\circ\text{C}$
$T_M = 1685 \text{ K}$
$\epsilon = 0.3$
$Pr = 0.023$
$Ma = 325 R\Delta T, \Delta T = T_H - T_M$

The Stefan-Boltzmann constant is $s = 5.668 \cdot 10^{-5} \text{ erg/cm}^2 \text{ s K}^4$, and the Prandtl number Pr and Marangoni number Ma are defined by

$$Pr = \frac{\nu}{K}, \quad Ma = \frac{R\gamma\Delta T}{\mu K}. \quad (15)$$

Another Marangoni number can be defined that is based on the temperature difference between the highest surface temperature T_{\max} and T_M . This Marangoni number, designated by $Ma^* = R\gamma(T_{\max} - T_M)/\mu K$, is not an independent parameter but part of the solution.

OUTLINE OF THE NUMERICAL PROCEDURE

The numerical solution of the initial-boundary value problem, defined by Eqs. (1) through (11), (13) and (14), is carried out with the aid of a finite-difference technique, boundary-fitted coordinates, and artificial compressibility. Details are given in Ohring and Lugt,²³ with applications to different flow problems.^{24,25} Thus, only an outline is given in this paper. Hsieh and Pline,²⁶ in a numerical scheme somewhat similar to the present one, also employ boundary-fitted coordinates and artificial compressibility. In addition, they use a third-order upwind scheme for the convective terms, whereas in this paper central differencing without added smoothing terms are used for the convective terms. Reviews^{27,28} on numerical methods for free boundaries also describe other possible methods.

For the numerical integration of this initial-boundary value problem it is convenient to make a boundary-fitted coordinate transformation. In the figures that follow, the origin of the z -coordinate is shifted to $-L/2$, that is, the new coordinate is $z' = z + L/2 = z + 0.5 \text{ cm}$. Figure 3a is a schematic drawing of the way in which the physical plane (z', r) is mapped onto the computational domain (ξ, η). Only the coordinate lines which form the boundaries of the two regions are drawn. The coordinate lines in physical space are mapped onto a uniformly spaced Cartesian mesh with a unit mesh spacing in each coordinate direction.

As the flow field evolves in time, the grid in physical space will move and its coordinate lines will be attracted to regions of high flow gradients through the use of an adaptive-grid technique. However, the Cartesian grid in computational space always remains fixed and uniform. This is the major advantage of using a mapping. The physical region is mapped onto a computational space with a Cartesian grid consisting of 161 points in the ξ -coordinate direction and 99 points in the η -coordinate direction. Total mass conservation at each time step is enforced by distributing any deficient or surplus amount evenly along the free surface. (It may be mentioned that the number of grid points used in this paper is almost two orders of magnitude greater than that of Ref. 13, a fact of particular importance for the accuracy of the solution at the free surface).

The curvilinear coordinates (ξ, η) are obtained as solutions of the two elliptic partial differential equations with the physical space coordinates (z, r) as independent variables

$$\xi_{rr} + \xi_{zz} = (\xi_r^2 + \xi_z^2) P^*(\xi, \eta) , \quad (16)$$

$$\eta_{rr} + \eta_{zz} = (\eta_r^2 + \eta_z^2) Q^*(\xi, \eta) . \quad (17)$$

P^* and Q^* are control functions.²³ Since all calculations are to be done in the rectangular computational domain, these two elliptic partial differential equations are transformed by interchanging the dependent and independent variables. As a result, the physical space coordinates (z, r) are solved in terms of the computational space coordinates (ξ, η) at each time step.²⁹

The continuity equation (1) is replaced by an equation with pseudo-compressibility for numerically conserving mass at each physical time step:

$$p_r + u_r + \frac{u}{r} + w_z = 0 . \quad (18)$$

τ is the pseudo-time. Mass conservation was excellent for all flow cases computed: Typically, the average value of $|\nabla \cdot \vec{v}|$ for the largest Marangoni number was between 10^{-4} and $10^{-3} s^{-1}$, except when the flow was disturbed by the moving heater. Then, the average value of $|\nabla \cdot \vec{v}|$ was between 10^{-3} and $10^{-2} s^{-1}$. These data may be compared with the maximum value of vorticity of $1350 s^{-1}$.

Altogether six partial differential equations for u , w , T , r , z , and p must be solved with the proper boundary conditions. The finite-difference technique for solving these equations is briefly described in the following way: All spatial derivatives, including one-sided derivatives at the boundaries, are replaced by finite-difference operators of second order in the computational space. The time-differencing procedure is implicit with a certain number of pseudo-time steps for each physical time step.

A "four-color" scheme (Fig. 3b) is used in the interior of the computational space. The use of such a scheme, which can be vectorized, resulted in an order of magnitude increase in computer speed on the Cray-XMP 2/16 and Cray-YMP 8/64 on which the computations were performed. The "four-color" scheme consists of obtaining updates for u and w at all the \circ points simultaneously, then at all the \blacksquare points, the \times points, and the Δ points, in that order. The latest available updates are used in this process. The "four-color" scheme is also applied to p and to T independently.

The computational cycle for one complete pseudo-time step iteration consists of (a) applying the "four-color" scheme to compute updates for r and z followed by obtaining the latest updates for r at successive points along the left and right boundaries; (b) obtaining updates for p at successive points along the boundaries from the boundary conditions for p followed by applying the "four-color" scheme to compute updates for p in the interior; and (c) obtaining updates for u and w at successive points along the boundaries from their boundary conditions, and then obtaining updates for h at successive points along the free surface from the kinematic condition (7), followed by applying the "four-color" scheme to compute updates for u and w in the interior.

At the completion of this computational cycle, after the latest updates for r , z , u , and w satisfy certain convergence criteria at all points, these updates are the solution at the new time level $n + 1$. If the convergence criteria are not met, cycle (a) through (c) is repeated until they are met. A new time step is considered computed when the corresponding components of the velocity fields of two consecutive iterations are within 1% of each other. The accuracy of a very similar numerical scheme was checked with fine grids.²³ It may be mentioned that the singularities at $r = R$, $z = \pm L/2$ diminish the efficiency of the numerical scheme considerably, but their range of influence on the whole flow field is only local.

Before the iterative process just described is used for obtaining r , z , u , w and p at time level $n + 1$, the temperature T at the new time level $n + 1$ is obtained by the same iterative method with the velocities u and w from time level n . Computations of the stream function are not presented in this paper. Therefore, the streamline pictures show only selected streamlines obtained numerically from the velocity fields. These selected streamlines do not represent equally spaced incremental values of the mass flux.

RESULTS

Three numerical calculations were performed for $Ma = 10,400, 30,225$, and $50,050$ with the constants of Table 1, with $R = L = 1 \text{ cm}$ and with $a = 10^{-4}$. The flow was disturbed for all three cases at $t = 1.52 \text{ s}$ by moving the heater from $z = 0$ to $z = 0.25 \text{ cm}$ at $t = 1.62 \text{ s}$ and back at time $t = 1.72 \text{ s}$.

Before the results are given, the following definitions and remarks are useful with regard to the graphical presentation of the data and their interpretation. An axisymmetric vortex ring is defined as a fluid motion with nested closed streamlines in the meridional plane (r, z) with reference to a frame fixed to the center of the streamlines.³⁰ In a steady flow, the reference frame is the coordinate system (r, z) itself. For the vorticity field in such a steady flow with closed streamlines, Prandtl's restriction³¹ holds that the integral over the viscous terms along closed streamlines vanishes

$$\nu \oint \text{curl } \vec{\omega} \cdot d\vec{s} = 0, \quad (19)$$

with $d\vec{s}$ the length element along the streamlines. Prandtl concluded that for almost frictionless motion, that is for an almost inviscid fluid motion with arbitrarily small ν but $\nu \neq 0$, the vorticity of an axisymmetric flow in the meridional plane inside a closed streamline must be

$$\omega_\phi = \text{const} \cdot r. \quad (20)$$

This result follows from Helmholtz's conservation law $d(\omega_\phi/r)/dt = 0$ for an axisymmetric inviscid fluid flow with $\nu = 0$ that yields for a steady-state flow

$$\frac{\omega_\phi}{r} = f(\psi). \quad (21)$$

ψ is the stream function. Eq. (20) is a special case of a maximum principle that holds for any steady axisymmetric motion of a *viscous* fluid: ω_ϕ/r can have an extremum only at the boundary.³² A vortex ring (characterized above by nested closed streamlines) in a steady flow is thus "attached" in the sense that its ω_ϕ/r - field has no extremum inside the flow region and that lines of constant ω_ϕ/r may at the most form "tongues." However, this vorticity field without extremum still must obey restriction (19).

Vortex shedding is an intrinsically time-dependent process when the tongues of ω_ϕ/r -lines pinch off and form closed lines. This means that an extremum of ω_ϕ/r has developed and that the vortex ring has "detached." Because of the importance of the ω_ϕ/r - field, vorticity is presented in the text that follows in the form of lines of constant ω_ϕ/r . Some examples of equivorticity lines, that is of lines of constant ω_ϕ , are also given for comparison. These lines are significant for the study of the flux of vorticity, defined by $\nu \partial \omega_\phi / \partial n$, with n the coordinate normal to the lines. That $\partial \omega_\phi / \partial n$ is relevant and not $\partial(\omega_\phi/r) / \partial n$ can be seen immediately in the example of the Poiseuille flow in a pipe, for which $\partial(\omega_\phi/r) / \partial n$ is zero at the wall but not $\partial \omega_\phi / \partial n$. However, for all practical purposes the flux inside the fluid can be discussed also with lines of constant ω_ϕ/r .

It may be mentioned that the center of nested closed streamlines, the location of extremum of ω_ϕ/r , and the location of extremum of ω_ϕ do not coincide in general. The results will show that the center of closed streamlines is closer to the location of extremum of ω_ϕ/r than to the location of extremum of ω_ϕ .

The Case $Ma = 10,400$

The Marangoni number $Ma = 10,400$ corresponds to a temperature difference $T_H - T_M$ of 32°C . Figure 4 shows lines of constant ω_ϕ/r at six different times (solid lines represent negative and dashed lines positive contours) prior to and after the asymmetric disturbance of the flow. After the heater is turned on at $t = 0$, immediately strong layers of vorticity along the free surface are generated by the surface shear stress that increase in strength toward the corners (which are formed by the walls and the free surface). Associated with the heater-generated surface shear stress is the occurrence of surface velocity which increases toward the corners, builds up in time, and reaches values up to 2.93 cm/s . This process is called *slamming*. The surface vorticity is forced away from the walls and deflected into the interior by forming tongues. This curling deflection of surface vorticity due to slamming creates wall vorticity of opposite sign that also forms tongues beneath. The flow situation is different from ordinary cavity flows in which the sign of the vorticity does not change at the corner, and a boundary layer along the entire solid wall develops.³³ In Fig. 4 no vortex shedding, that is, no extremum of ω_ϕ/r , is observed. At $t = 10.5 \text{ s}$ the flow reaches an almost steady state. The enlarged core of the right roll is displayed in Fig. 5 which shows lines of constant ω_ϕ/r indicating a smooth transition from high corner values to zero at the center point $r = 1, z' = 0.5 \text{ cm}$. Thus, the maximum principle for ω_ϕ/r is obeyed; the roll is "attached." For comparison, Fig. 6 demonstrates the occurrence of extrema of ω_ϕ and hence the unsuitability of the ω_ϕ - field to distinguish between steady state and shed vortices. In Fig. 7 the surface vorticity $(\omega_\phi)_s$ is displayed which is equal to the negative shear stress at the surface. Since this free surface is barely deformed (that agrees with Kazarinoff and Wilkowski's findings¹³), the surface vorticity can be checked, for the computed T_z given, with Eq. (12) for a flat surface. The agreement is so good that the two curves, shown in Fig. 7 for the times 1.00 s , 1.72 s , and 10.5 s , are indistinguishable, except at the extrema near the wall. Surface vorticity increases with time near the walls. The tongues formed by the surface and wall vorticity prevent the two toroidal convection rolls to occupy the whole float zone and confine the main fluid motion to the surface region. The streamlines in Fig. 8 show these rolls with the flow direction from warmer to cooler parts of the free surface. The center of the rolls moves slightly toward the symmetry line $z' = 0.5 \text{ cm}$ but stays close to the free surface. At almost steady state $t = 10.5 \text{ s}$, two additional rolls beneath the main ones occur (they have been observed already at $t = 7.5 \text{ s}$ but not shown in Fig. 8).

The isotherms in Fig. 9 reveal that the temperature gradient at the cold walls increases with time but is unevenly distributed along the walls. This means that the heat transfer from the liquid to the solid phase increases with time but much more near the free surface. This will be verified quantitatively further below. The temperature at the free surface itself, that is the difference $(T_s - T_M)^\circ\text{C}$, is plotted in Fig. 10a for times before the disturbance is imposed. The curves end at the cold wall at a nonzero angle. The corner points ($r = 1, z' = 0$ and 1 cm) are thus singular. The values of the Marangoni number Ma^* are 230 at $t = 0.50 \text{ s}$, 268 at $t = 1.0 \text{ s}$, and 278 at $t = 1.52 \text{ s}$.

Despite the strong disturbance imposed at $t = 1.52 \text{ s}$, there is no tendency toward instability. The flow field returns quickly to an almost steady state as demonstrated in Fig. 11 where the surface vorticity at $z' = 0.5 \text{ s}$ is plotted against time. A tiny damped oscillation is visible that is negligible if one considers that at $t = 4.0 \text{ s}$ the amplitude is less than 2% of the maximum surface vorticity. The lines of constant ω_ϕ/r in Fig. 4 at $t = 10.5 \text{ s}$ display symmetric tongues except for the lowest level of vorticity of the order one s^{-1} . This asymmetry appears only at a level of less than 2% of the maximum surface vorticity which

reaches a value of $|(\omega_\phi)|_s = 140 \text{ s}^{-1}$ (Fig. 7). The surface velocity w_s for $t = 10.5 \text{ s}$ is given in Fig. 12 and reveals complete symmetry.

The temperature fields in Fig. 9 change barely after the disturbance except for a thin layer along the free surface as shown in Fig. 10b. From $t = 7.5 \text{ s}$ on the surface temperature is symmetric around $z' = 0.5 \text{ cm}$ and the two curves for $t = 7.5 \text{ s}$ and $t = 10.5 \text{ s}$ coincide completely with a maximum surface temperature difference of $T_s - T_M = 0.80$ which corresponds to a value of $Ma^* = 260^\circ\text{C}$. This coincidence confirms that the fluid motion is at an almost steady state. The result does not agree with Kazarinoff and Wilkowki's finding¹³ that instability should occur at a Marangoni number of $Ma = 1202$. In this context it may be mentioned that symmetric initial solutions should remain symmetric in time with an accurate numerical scheme and should only develop asymmetrical patterns after an asymmetric disturbance is imposed.

The Case $Ma = 50,050$

The second case with $Ma = 50,050$ corresponds to a temperature difference of 154°C . As in the previous case, the heater was turned on at $t = 0$ in a symmetric position and then, at $t = 1.52$, the heater was moved out of this symmetric position and back to create an asymmetric disturbance of the flow field. Lines of constant ω_ϕ/r , surface vorticity, and streamlines are shown in Figs. 13 through 16, and isotherms and surface temperature in Figs. 18 and 19 for the period from $t = 1.50 \text{ s}$ to 4.00 s .

As expected, the slamming of the flow near the surface against the cold walls is larger, compared to the flow of the lower Marangoni number. The core of the rolls is wider (Fig. 13), and curved tongues of vorticity from the free surface fill out the core, without forming closed ω_ϕ/r - lines before the disturbance (Fig. 14, $t = 1.5 \text{ s}$). Fig. 15 shows the magnitude of the surface vorticity which reaches a value of 1200 s^{-1} at $t = 2.5 \text{ s}$. Maximum surface velocities of about 10 cm/s occur. The two additional weak toroidal rolls beneath the main rolls develop earlier than for $Ma = 10,400$ (Fig. 16).

The disturbance imposed causes now an asymmetric pair of rolls and permanent oscillation. The rolls have extrema of ω_ϕ/r as seen in Fig. 14, $t = 2.5 \text{ s}$, indicating *detached* rolls. Compared to attached vortices characterized by vorticity tongues only, detached vortices have a larger moment of inertia due to higher core rotation. The way detached rolls increase and then maintain the oscillation of the float zone for $Ma = 50,050$ will be explained in detail below. It suffices here to demonstrate the undamped oscillation. In Fig. 17 the surface vorticity at $z' = 0.5 \text{ cm}$ and $z' = 0.0125 \text{ cm}$ is plotted against time. The amplitude increases and approaches a constant value. The frequency of the oscillations is 0.27 Hz and is constant over the time span computed.

Isotherms and surface temperature are plotted in Figs. 18 and 19. Major changes in the temperature field occur only in a layer adjacent to the free surface. The surface itself deforms on a "microscopic" scale which is of the order of 10^{-4} cm , in fair agreement with Kazarinoff and Wilkowski.¹³

The last two cycles from $t = 25 \text{ s}$ to $t = 34 \text{ s}$ have almost constant amplitude, and their behavior is recorded in Figs. 20 through 29. Lines of constant ω_ϕ/r in Figs. 20 and 21 and equivorticity lines in Fig. 22 reveal the oscillatory behavior of the flow field in the form of rolls of pulsating size. The main activity is restricted to the upper half of the float zone near the free surface. The corresponding surface vorticity, surface velocity, streamlines, isotherms, and surface temperature are plotted respectively in Figs. 23 through 27.

A close-up of the core region of the rolls in Fig. 21 is being used now to describe the cyclic change of the float zone. During the transient phase, each of the two rolls has established a core of vorticity with extreme values (visible as nested closed ω_ϕ/r -lines except at certain transition phases). This local extremum assumes maxima and minima during a cycle representing periods of accelerating and decelerating core rotation. The alternating build-up and decay of the rolls is accompanied by vorticity flux, changing its direction and visible in the form of retreating and advancing vorticity tongues and closed lines as well. The direction of the flux in the right core is indicated by arrows in Fig. 21. A comparison with equivorticity lines in Fig. 22 again demonstrates that ω_ϕ/r - lines are better suited for displaying the flow characteristics than ω_ϕ - lines. Notice the occurrence of two extrema in Fig. 22 at $t = 27, 28$, and 30 s.

The processes involved are described now in detail. To begin with, the flow field at $t = 28$ s in Fig. 21 is chosen when the largest displacement of the flow (that is, the largest amplitude) from the "symmetric" flow configuration occurs. The right roll has almost attained its smallest size associated with a maximum of $|\omega_\phi/r| \approx |-47| \text{ cm}^{-1}\text{s}^{-1}$ at the core's center. The roll on the left side, in contrast, has acquired its largest extension and is approaching its minimum of positive ω_ϕ/r . The surface temperature has its highest value in this left half of the float zone (Fig. 27) and provides maximum surface vorticity and slamming (Figs. 23 and 24). Surface vorticity is now pouring into the center and is filling up the core (Fig. 21, $t = 29$ s). This means that the rotation of the left roll increases and the roll contracts. This process takes place in concert with the right roll which expands through decay, that is, through diffusion of center vorticity. An instant will be reached ($t = 30$ s), at which the left roll has shrunk to its minimum; the center vorticity of the left roll has leveled and closed lines vanish (Fig. 14, $t = 4.0$ s shows also such an instant). At the free surface, meanwhile, the location of zero vorticity shifts to the right because of the strengthening of surface vorticity on the left side. This, in turn, causes the shift of maximum surface temperature to the right since zero surface vorticity and maximum surface temperature are tied together (Fig. 27). Thus, despite the symmetric position of the ring heater, the location of maximum surface temperature depends on the fluctuating flow field. After $t = 30$ s the process repeats itself with exchanged roles.

Based on this description of the pulsating core region, the following explanation is offered. About $t = 28$ s (Fig. 21), the right roll shrinks to a concentrated vortex. The thin feeding layer of vorticity, beginning at the corner and surrounding the core, strengthens through contraction. At the same time the left roll expands; the surrounding feeding layer is stretched and weakened. The combined action of the two vorticity layers at the surface causes the location of $\omega_s = 0$, that is $(T_s)_{\max}$, to move to the left. The maximum displacement is reached at about $t = 28$ s (Fig. 29), when the build-up and emptying of the two rolls, respectively, have ceased. Then, the process is reversed (Fig. 21, $t = 29$ s). The restoring mechanism, which tries to re-establish the symmetric flow situation (zero amplitude), consists now of contracting the left roll and of stretching the right roll. This restoring mechanism is supported by a maximum input of surface vorticity at the left corner. At $t = 29$ s, zero amplitude occurs with an overshoot that is visible in the non-symmetry of the flow (Fig. 21) and caused by the moment of inertia of the rolls. The analogy to a swinging pendulum is at hand.

It becomes clear now what happens during the transient phase after the heater has briefly been moved to the right and back. At $t = 1.72$ s, the right roll is about to form closed vorticity lines with the largest rotation next to the the center, while the left roll has still the feature of an attached vortex (not shown in Fig. 14). At $t = 2.5$ s in Fig. 14, the

right roll has clearly established itself as a detached vortex with closed loops and with vorticity pouring into the center. The left roll is weaker but occupies yet about the same space as the right roll. The stronger right roll has pushed $(T_s)_{\max}$ a little into the left half. At $t = 4.0$ s the reverse situation is seen. With each cycle, a larger body of fluid gets involved in the oscillation. The expanding roll requires more space and squeezes the other roll which in turn gets more concentrated. This process is supported by the simultaneous larger shift of $(T_s)_{\max}$ away from the symmetry line $z = 0$. The amplitude of the oscillation increases until the vorticity gradients in and around the cores become so large that diffusion takes over. It is remarkable that the frequency of the oscillation during the transient period remains constant.

The growth and maintenance of oscillation for $Ma = 50,050$ is in contrast to the flow situation for $Ma = 10,400$. Here, the asymmetrically disturbed flow near the surface is immediately damped by diffusion and the core regions of the roll barely affected (Fig. 4). There is a certain analogy of the onset of instability and the maintenance of the oscillating float zone with the symmetry breaking of a parallel flow behind a circular cylinder. A steady symmetric flow with attached vortices changes at a critical Reynolds number to a periodic vortex street with detached vortices. It may be mentioned that at the same Reynolds number beyond the critical one the two (unstable) attached vortices of the steady-state configuration are weaker than the shed vortices of the (stable) unsteady configuration. The latter one is apparently more energy-efficient than the steady flow. In the case of the float zone, heat transfer from the surface to the walls appears to be more efficient with detached oscillating rolls.

The instantaneous streamline patterns in Fig. 25 support the scenario described. Something novel is being observed: Rolls near the free surface can extend toward the axis and can spawn weak rolls within a single closed streamline. The weak rolls are indicated by one or two streamlines only. It should be emphasized again that the streamlines do not represent equally spaced incremental values of the mass flux. It is noteworthy, that the streamline patterns cannot expose the subtleties of the core's vorticity field that reveal the mechanism of oscillation.

Isotherms are given in Fig. 26. The oscillatory change of the temperature field affects the whole float zone, including the axis $r = 0$. The temperature oscillation in the upper half is clearly governed by convection. In contrast, fluid motion near the axis is virtually absent, and the temperature change can only take place by diffusion. The patterns of isotherms next to the cold walls reveal that the change of the temperature gradient along the walls is larger than that for a steady-state flow and oscillating (Fig. 28). This greater change confirms the statement made in the introduction that the solidification of molten silicon in an oscillating float zone would take place in a more uneven way than that in a float zone with steady convection. The surface temperature is plotted in Fig. 27. During the oscillation period the maximum temperature difference remains approximately 3°C but its location switches back and forth. The periodic change of the slope of the curves at the corner is large, indicating periodic slamming. Fig. 27 also shows that the surface temperature is almost constant at the symmetry point $z' = 0.5$ cm, that is, $T_s - T_M = 2.9^\circ\text{C}$. This value corresponds to $Ma^* = 943$. A comparison of Nusselt number with radiation number reveals that the latter is one thousand times smaller.

Finally, computations were made with the assumption of a flat free surface, that is, with $h = R$. This assumption was introduced at $t = 26$ s by abruptly changing the boundary conditions (7) through (10) and (13) to

$$u = 0 , \quad (22)$$

$$p - 2\mu u_r = \frac{\sigma_M}{R} - \sigma_r , \quad (23)$$

$$\mu w_r = \sigma_z , \text{ or } \mu \omega_\phi = \gamma T_z , \quad (24)$$

$$\frac{1}{R_1} + \frac{1}{R_2} = -\frac{1}{R} , \quad (25)$$

$$-kT_r = \alpha(T - \theta) + s\epsilon(T^4 - \theta^4) . \quad (26)$$

Although the actual free-surface deformation is small (of the order of 10^{-4} cm), the combined or cumulative effect of "symmetrization" of the free-surface conditions due to the flat-surface assumption causes a damping of the disturbance (Fig. 30). Symmetrization means that the terms in Eqs. (7) through (10) and (13), which drop out due to $h_z = 0$, are also terms which contribute to asymmetric behavior: Constant $h = R$, Eq. (25), and vanishing $u = 0$, Eq. (22), obviously have a symmetrization effect. Although less obvious, the same is true for the pressure at the singular points $R = 1$ cm, $z = \pm 1/2$ cm, where the flat free surface condition enforces $p = \sigma_M/R$. On a deformable free surface, no symmetry at and near the singular points occurs, and the pressure fluctuates. Also temperature and temperature gradient, Eqs. (24) and (26), are affected by the assumption of a flat surface. Near the singular points, the term $|h_z T_z|$ in Eq. (13) is larger than the term $|T_r|$, which is zero exactly at the singular points. On a flat surface, vanishing $|h_z T_z|$ near the singular points make the temperature distribution more symmetric. This behavior influences the vorticity distribution along the free surface, Eq. (24), in such a way that the location where $\omega_\phi = 0$ moves closer to the symmetry plane $z = 0$ and with it T_{\max} . The oscillation thus diminishes. It is concluded that damping appears to be a combined or cumulative effect of the symmetrization of all free-surface boundary conditions.

Damping of the disturbance means that the oscillatory mode of the fluid motion changes with time to a steady mode. This result confirms the findings of Kamotani *et al.*¹² and Kazarinoff and Wilkowski¹³ that a deformable free surface is a necessary (but not sufficient) condition for the float zone to become unstable.

The Case $Ma = 30,225$

In order to narrow in on the critical Marangoni number, a third case between $Ma = 10,400$ and $50,050$, that is, $Ma = 30,225$, was chosen and computed. The results show also oscillations and thus instability. This means, that the critical Maragoni number must lie in the interval $10,400 < Ma < 30,225$. The frequency of the oscillations is 0.22 Hz, and Ma^* at the center is about $Ma^* = 618$. All other features of the oscillating motion, described for $Ma = 50,050$, are observed here too and are qualitatively the same.

CONCLUSIONS

The two main results of this paper are (1) the existence of a critical Ma -number between $10,400$ and $30,225$, at which the steady flow field becomes unstable and changes to an axisymmetric oscillatory field. An explanation for this oscillation is given. (2) A deformable free surface, even a minute one, is necessary for the onset of instability. These findings confirm those by Kazarinoff and Wilkowski,¹³ although quantitative differences exist with regard to the value of the critical Marangoni number. It is conjectured that the reason

for damping is the symmetrization effect of the boundary conditions for a flat free surface.

Both the steady-state solution at $Ma = 10,400$ and the oscillatory ones at $Ma = 30,225$ and $50,050$ consist of two toroidal rolls along the free surface and two very weak ones beneath. The essential fluid motion takes place in the upper half of the float zone near the free surface. The transient phase after the start of the heating process is practically finished in less than two seconds whereas the transient oscillatory motion needs more than 30 seconds. For $Ma = 50,050$ the frequency of the oscillation is 0.27 Hz , for $Ma = 30,225$ slightly lower, that is, 0.22 Hz .

The explanation for the onset of instability and the subsequent maintenance of axial oscillation is sought in the transition from attached rolls to detached rolls with increasing heat energy at a critical Marangoni number. Oscillation is established from an initial disturbance by pulsating rolls whose restoring mechanism is the build-up and decay of core vorticity supported by the oscillating location of highest surface temperature. The overshoot at the symmetry position is due to the large moment of inertia of the detached rolls and overcomes diffusion until a quasi-steady state with constant amplitude is reached. The flow quantity which is best suited as an indicator for instability and as a descriptor of the pulsating flow process is ω_ϕ/r and not ω_ϕ .

The free surface deforms only slightly of the order of 10^{-4} cm in agreement with Kazarinoff and Wilkowski's result.¹³ The velocity at the free surface is very high and reaches values of 11 cm/s for $Ma = 50,050$.

The whole temperature field oscillates and causes uneven heat transfer at the walls that is not desired for silicon crystal growth. It is thus confirmed that oscillating float zones should be avoided in engineering applications.

ACKNOWLEDGMENTS

The authors thank Dr. J. C. Duh, NASA Lewis Research Center, for his advice throughout the course of this research and Messrs. M. Hurwitz and R. Van Eseltine, Carderock Division, NSWC, for their valuable support. Thanks are also due to Mr. J. Tuccillo, Cray Research, Inc., for generously providing computer time.

REFERENCES

- [1] Chun, C.H. and W. Wuest, *Acta Astron.*, **5**, 1073 (1979).
- [2] Schwabe, D. and A. Scharmann, *J. Cryst. Growth*, **46**, 125 (1979).
- [3] Smith, M.K., *J. Fluid Mech.*, **166**, 245 (1986).
- [4] Sarma, G.S.R., *PCH Physico-Chemical Hydrodynamics*, **6**, 283 (1985).
- [5] Dressler, R.F. and N.S. Sivakumaran, *J. Cryst. Growth*, **88**, 148 (1988).
- [6] Ostrach, S., *Ann. Rev. Fluid Mech.*, **14**, 313 (1982).
- [7] Linde, H., *Convective Transport and Instability Phenomena*, edited by J. Zierep and H. Oertel, Jr., Braun, Karlsruhe, pp. 265-296 (1982).
- [8] Preisser, F., D. Schwabe, and A. Scharmann, *J. Fluid Mech.*, **126**, 545 (1983).
- [9] Schwabe, D., *Crystals: Growth, Properties and Application*, edited by H.C. Freyhardt, Springer, **11**, pp. 75-112 (1988).

- [10] Young, G.W. and A. Chait, *J. Cryst. Growth*, **96**, 65 (1989).
- [11] Roux, B., editor, GAMM Workshop, *Notes on Numerical Fluid Mechanics*, Vol. 27, Vieweg, Braunschweig, (1990).
- [12] Kamotani, Y., S. Ostrach, and M. Vargas, *J. Cryst. Growth*, **66**, 83 (1984).
- [13] Kazarinoff, N.D. and J.S. Wilkowski, *Phys. Fluids A*, **1**, 625 (1989).
- [14] Chun, C.H., *Acta Astron.*, **11**, 227 (1984).
- [15] Velten, R., D. Schwabe, and A. Scharmann, *Phys. Fluids A*, **3**, 267 (1991).
- [16] Kazarinoff, N.D. and J.S. Wilkowski, *Phys. Fluids A*, **2**, 1797 (1990).
- [17] Zebib, A., G.M. Homsy, and E. Meiburg, *Phys. Fluids*, **28**, 3467 (1985).
- [18] Fowles, W.W. and G.O. Roberts, *J. Cryst. Growth*, **74**, 301 (1986).
- [19] Rupp, R., G. Müller, and G. Neumann, *J. Cryst. Growth*, **97**, 34 (1989).
- [20] Shen, Y., G.P. Neitzel, D.F. Jankowski, and H.D. Mittelman, *J. Fluid Mech.*, **217**, 639 (1990).
- [21] Neitzel, G.P., C.C. Law, D.F. Jankowski, and H.D. Mittelman, *Phys. Fluids A*, **3**, 2841 (1991).
- [22] Levich, V.G. and V.S. Krylov, *Ann Rev. Fluid Mech.*, **1**, 293 (1969).
- [23] Ohring, S. and H.J. Lugt, David Taylor Research Center, Report DTRC-89/013, Bethesda, Md. (1989).
- [24] Ohring, S. and H.J. Lugt, *J. Fluid Mech.*, **227**, 47 (1991).
- [25] Lugt, H.J. and S. Ohring, *J. Fluid Mech.*, **236**, 461 (1992).
- [26] Hsieh, K.-C. and A.D. Pline, AIAA-paper 91-1306 (1991).
- [27] Yeung, R.W., *Ann. Rev. Fluid Mech.*, **14**, 395 (1982).
- [28] Floryan, J.M. and H. Rasmussen, *Appl. Mech. Rev.*, **42**, 323 (1989).
- [29] Thompson, J.F. and S.P. Shanks, Mississippi State University Report MSSU-EIRS-ASE-77-4 (1977).
- [30] Lugt, H.J., *Vortex flow in nature and technology*, Wiley, New York (1983).
- [31] Prandtl, L., *Verh. III. Intern. Math. Kongress*, Heidelberg, 484 (1904).
- [32] Lugt, H.J., *Am. J. Phys.*, **53**, 649 (1985).
- [33] Burggraf, O.R., *J. Fluid Mech.*, **24**, 113 (1966).

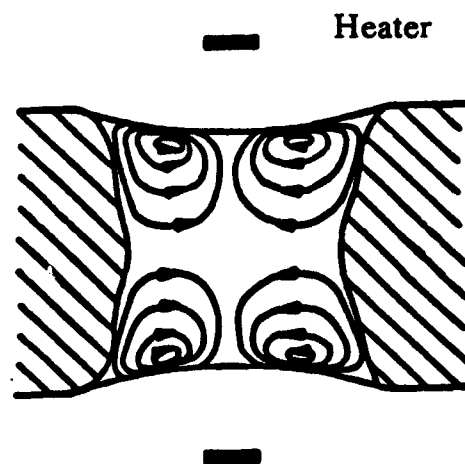


Fig. 1. Sketch of a float zone with streamlines and ring heater after Schwabe et al. (1978).

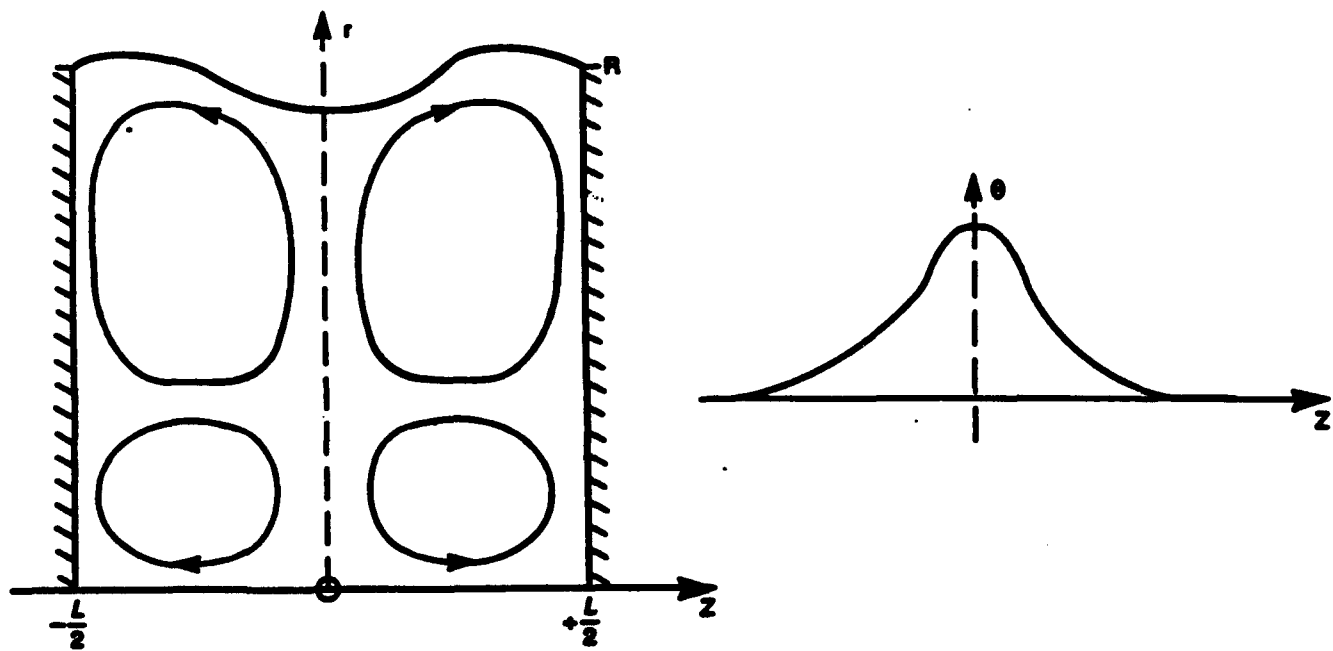


Fig. 2. Model of the float zone with temperature distribution of the ring heater.

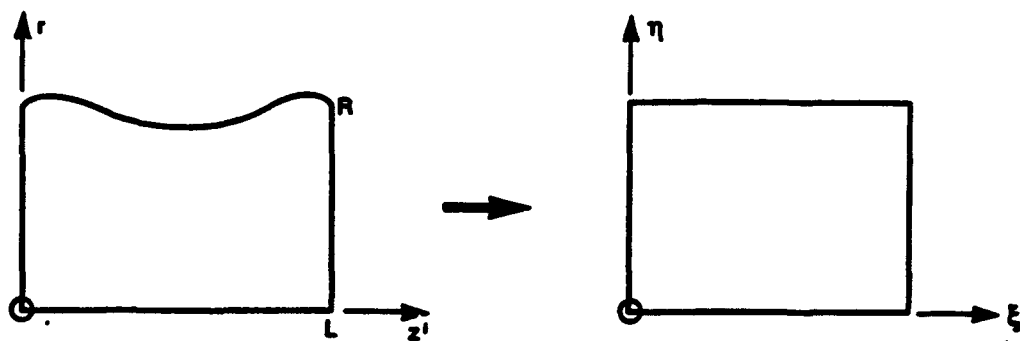


Fig 3a. Mapping of the physical plane (r, z') onto the computational plane (ξ, η)

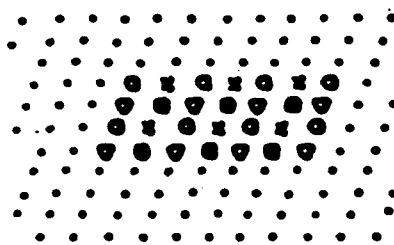


Fig 3b. "Four-color" scheme.

Fig. 3. Numerical grid layout.

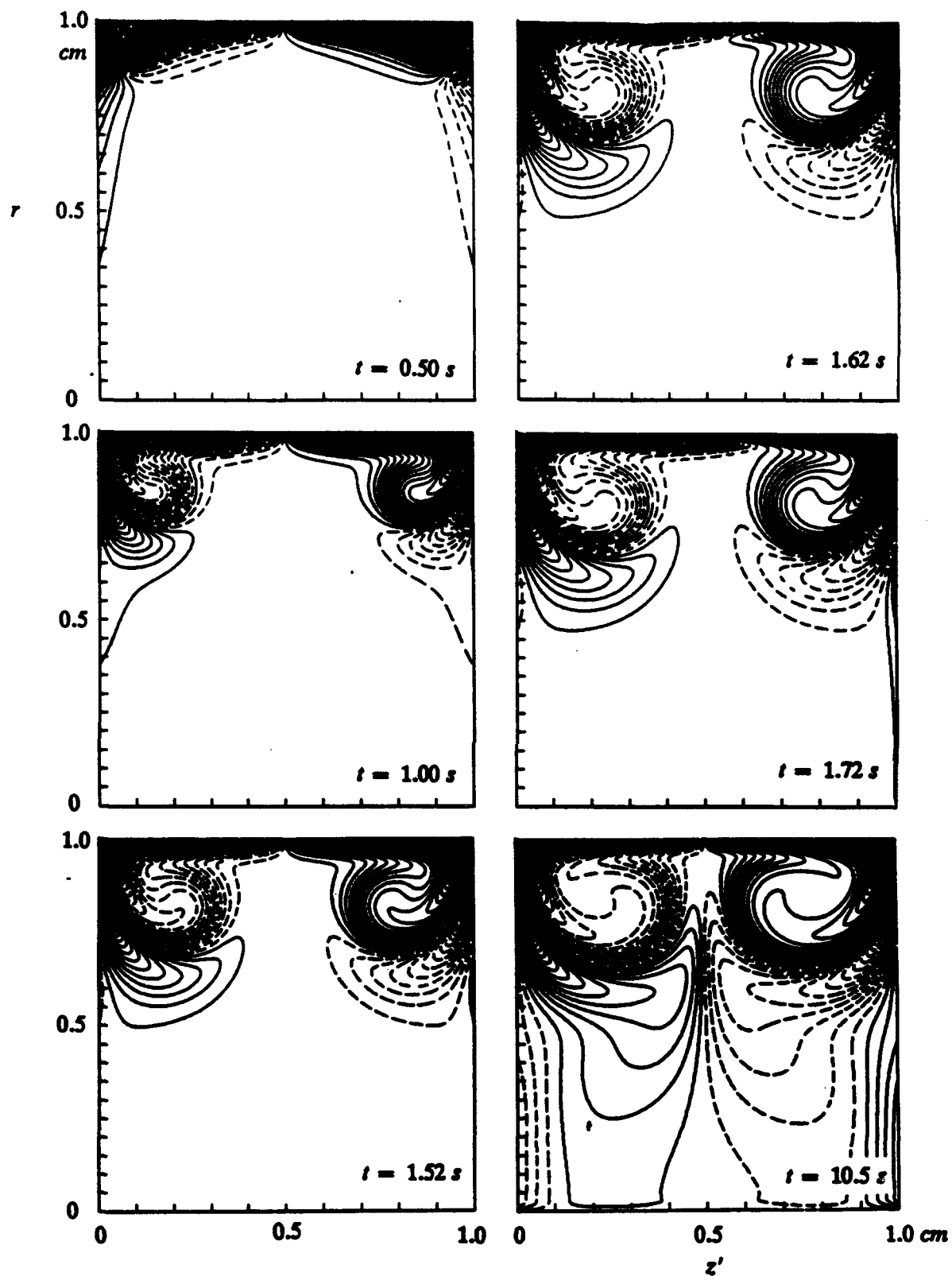


Fig. 4. Lines of constant ω_p/r for $Ma = 10,400$ at six different times. The ω_p/r -contours are ..., -3, -1, 1, 3,

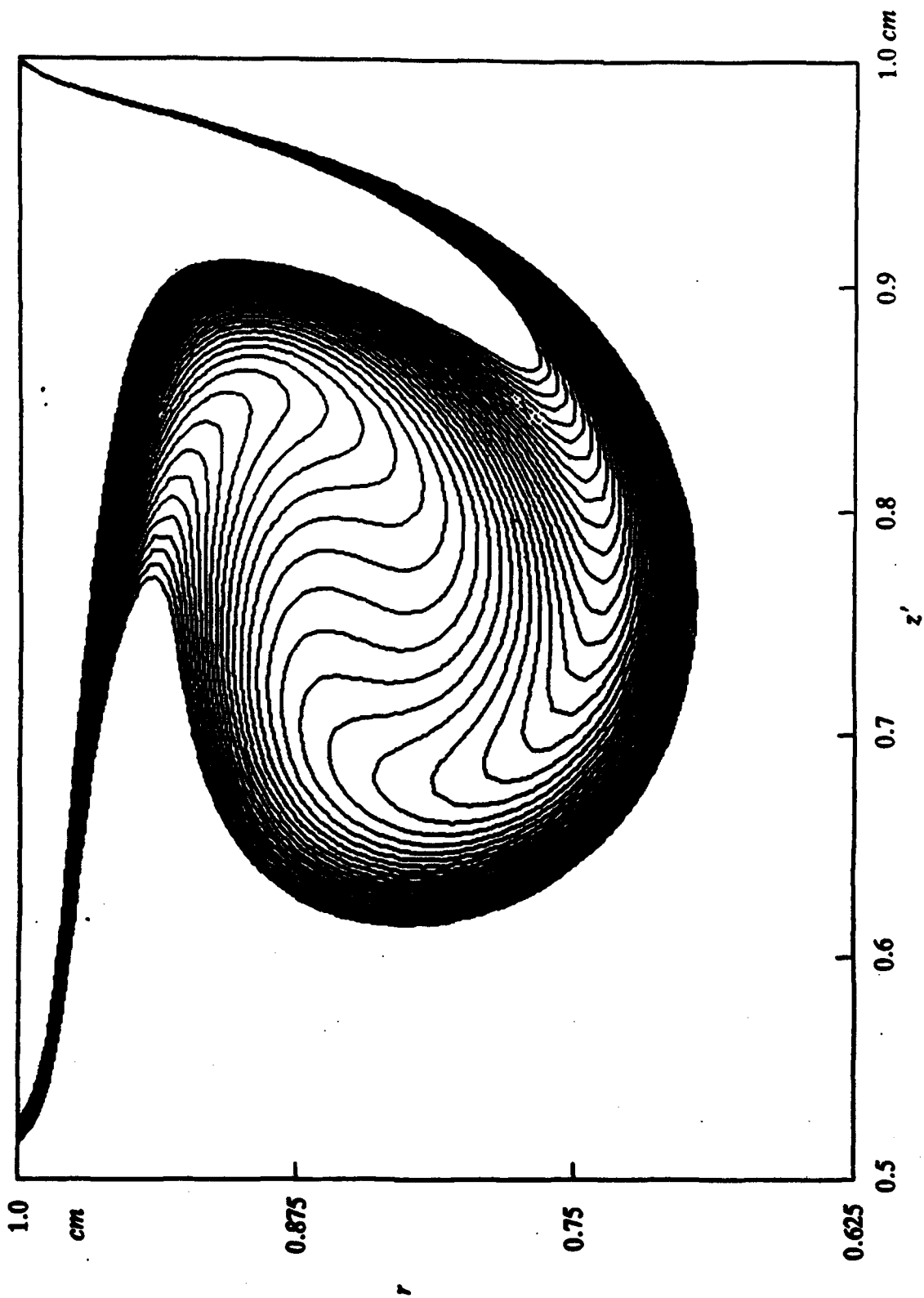


Fig. 5. Close-up of lines of constant ω_4/r for $Ma = 10,400$ in the core region of Fig. 4, $t = 10.5$ s. The ω_4/r - contours are $-23, -22.8, \dots, -15$.

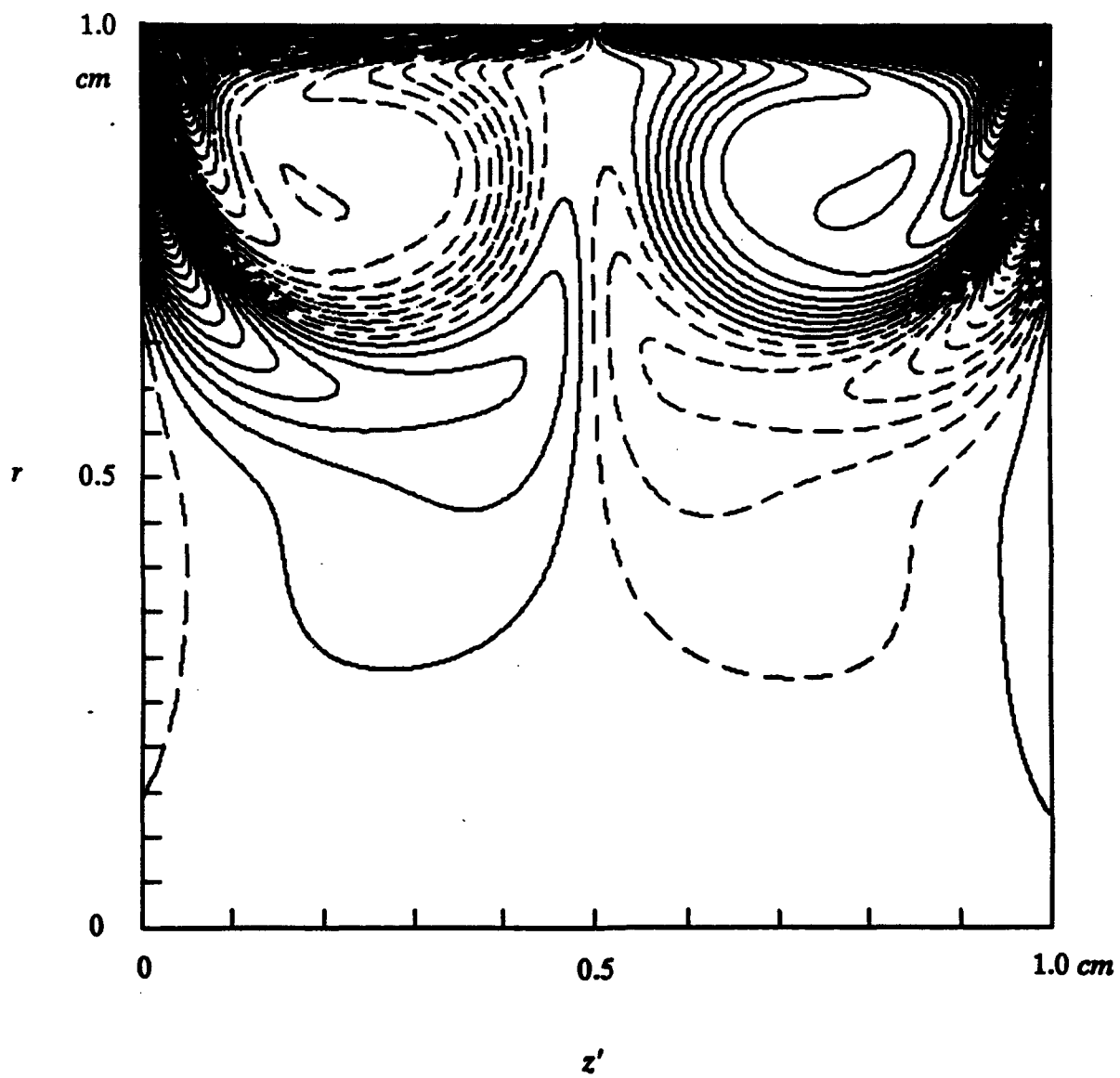


Fig. 6. Equivorticity lines (lines of constant ω_ϕ) for $Ma = 10,400$ at $t = 10.5$ s. The ω_ϕ - contours are $\dots, -3, -1, 1, 3, \dots$.

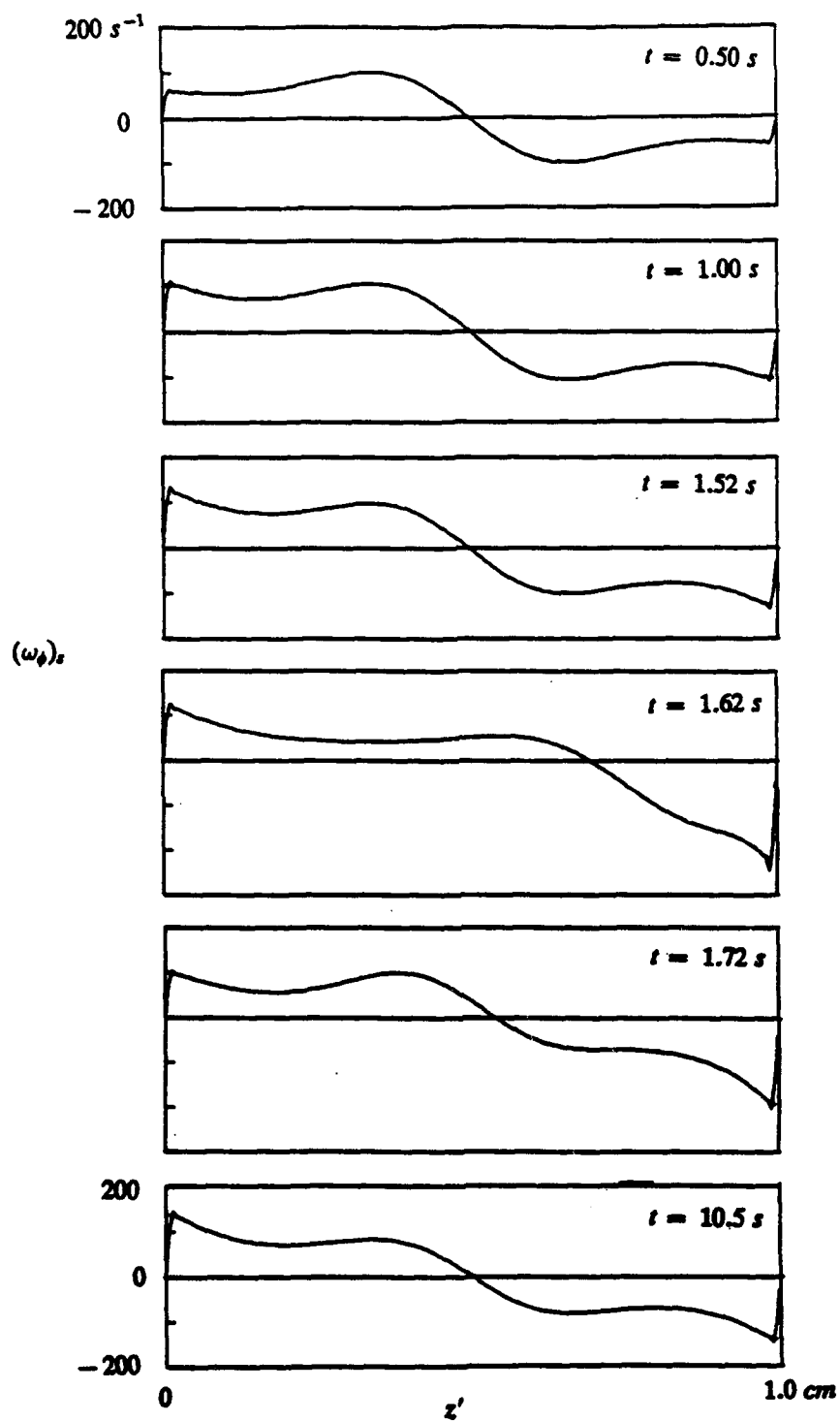


Fig. 7. Surface vorticity (= negative surface shear stress) for $Ma = 10,400$ of the vorticity field in Fig. 4.

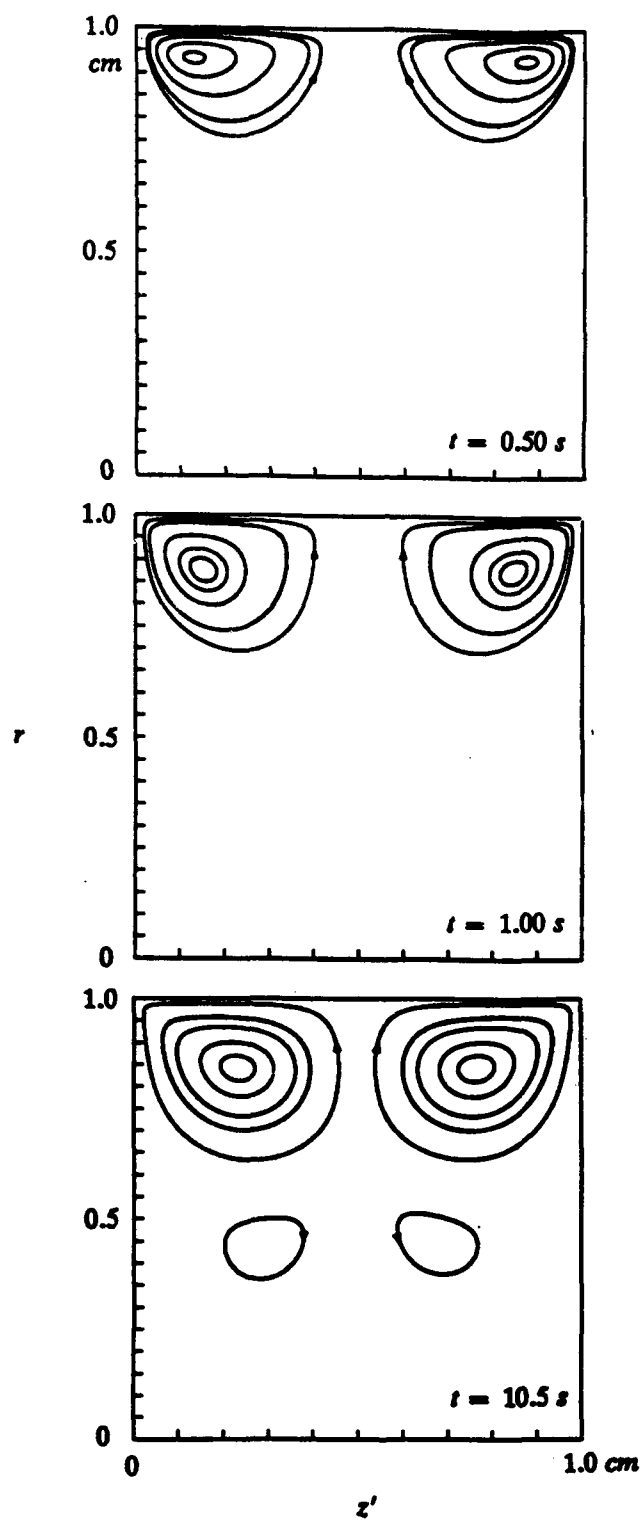


Fig. 8. Streamlines of the vorticity field in Fig. 4 at three different times.

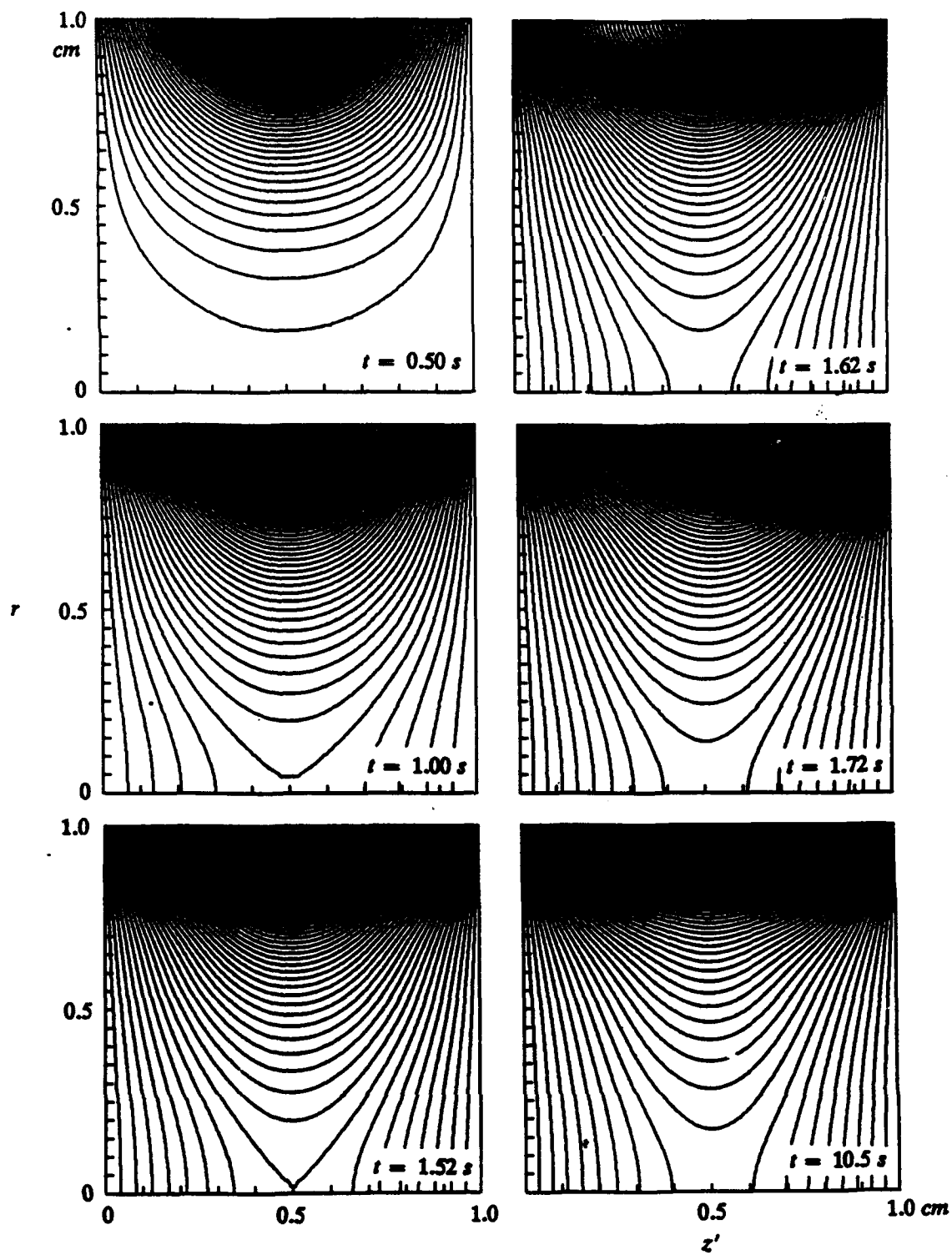


Fig. 9. Isotherms for $Ma = 10,400$ at six different times. The $T - T_M$ - contours are 0.01, 0.02, 0.03, ...

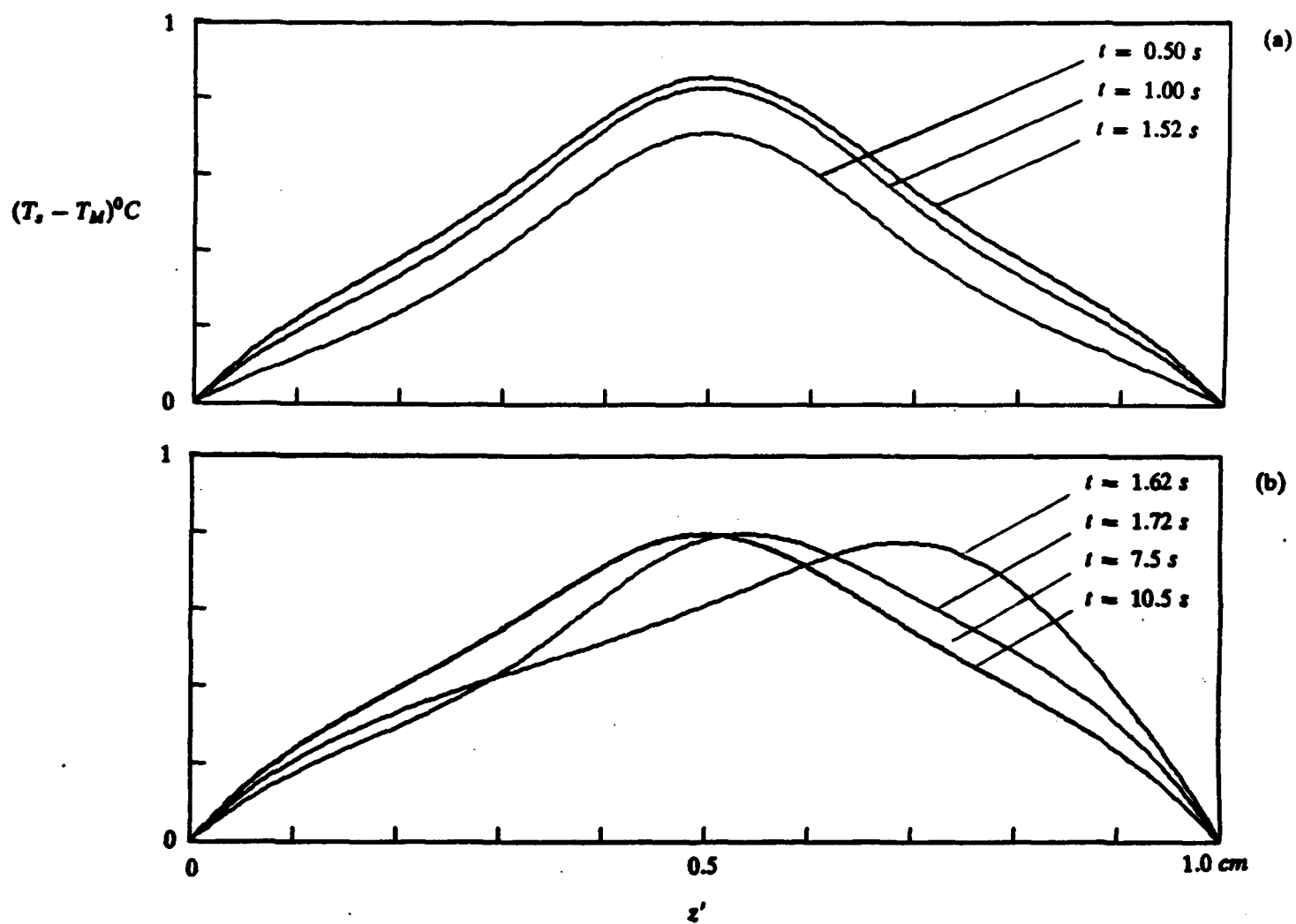


Fig. 10. Surface temperature for $Ma = 10,400$ of the temperature field in Fig. 9. (a) Before and (b) after the disturbance.

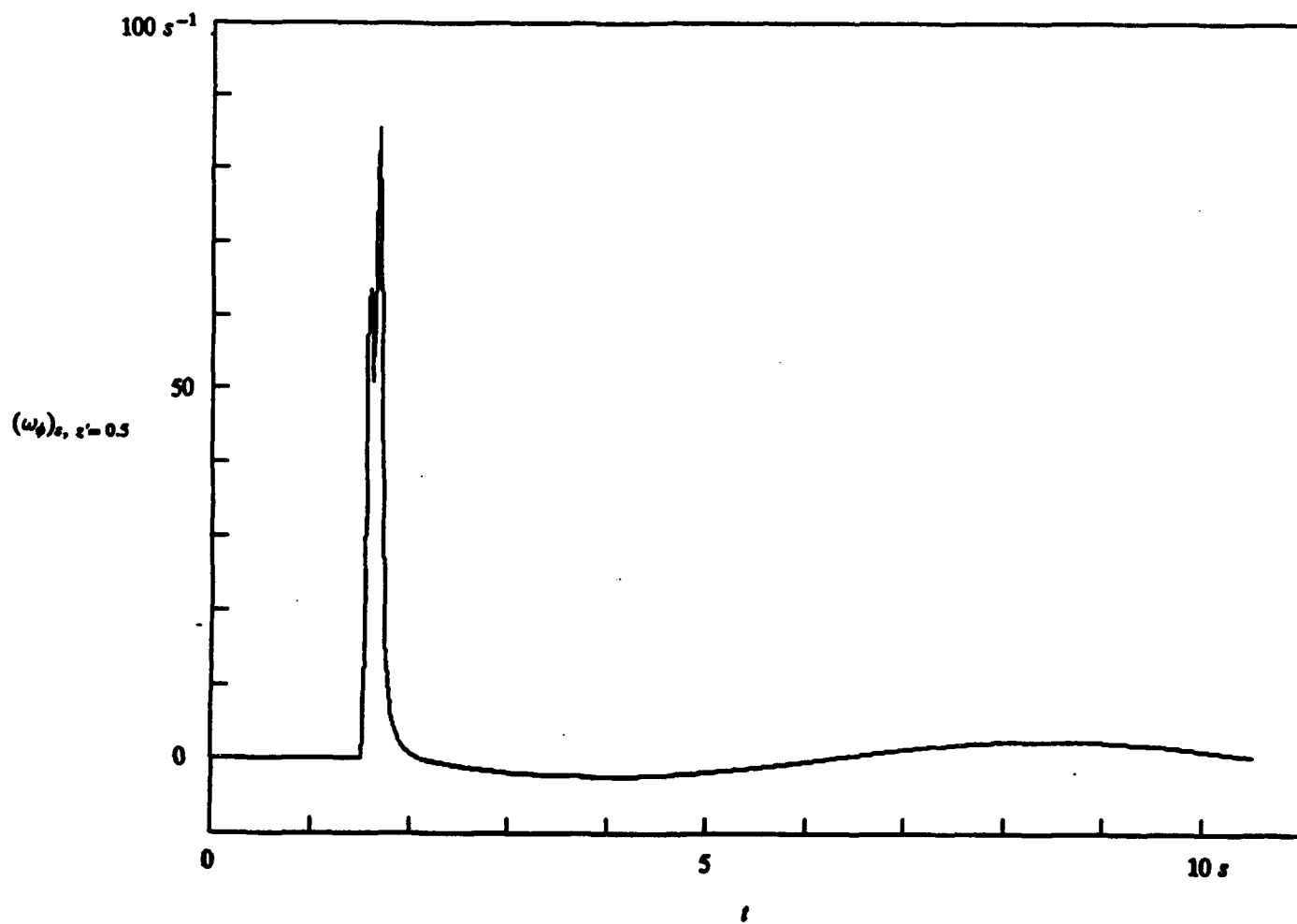


Fig. 11. Surface vorticity for $Ma = 10,400$ at $z = 0$ as a function of time.

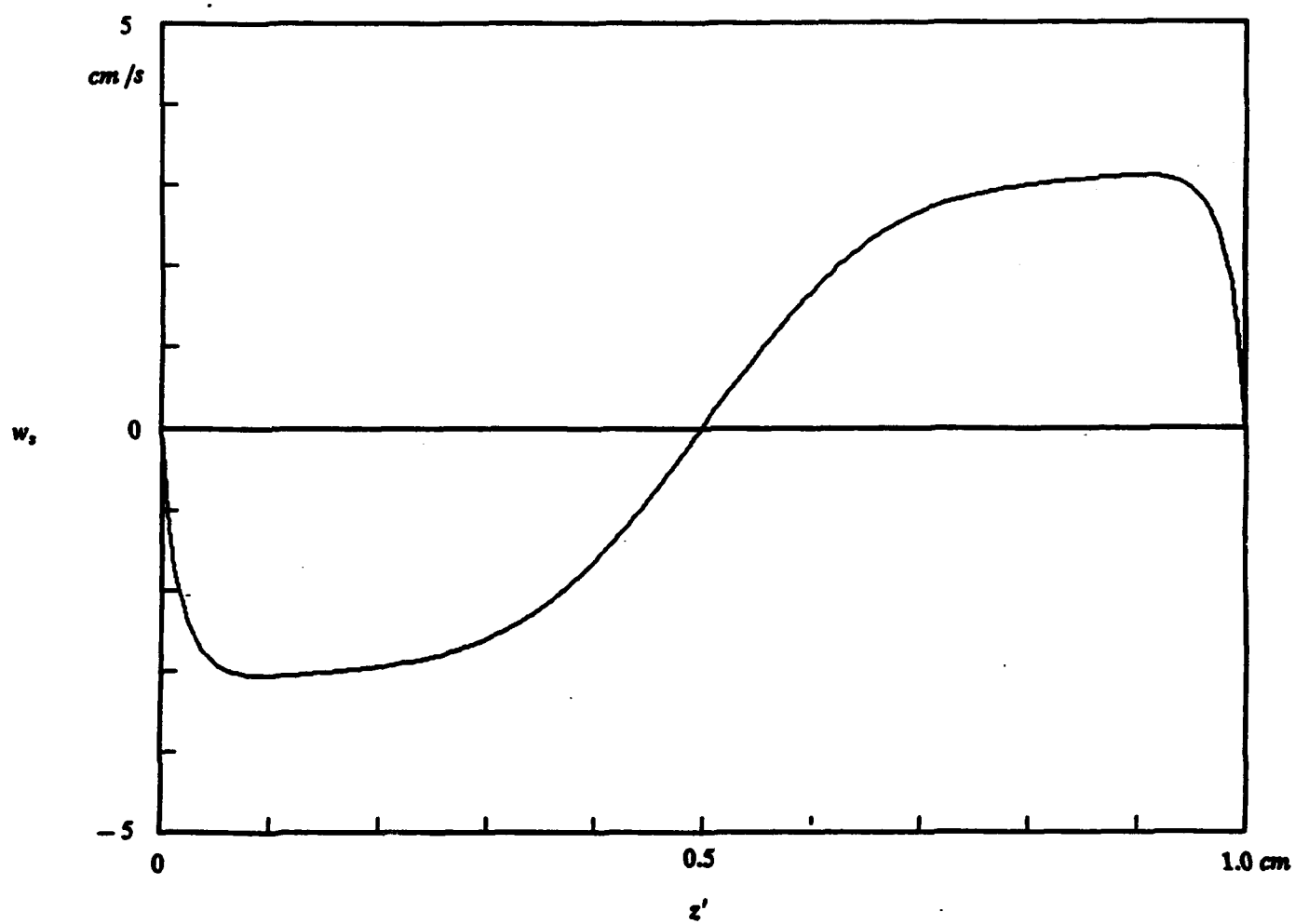


Fig. 12. Surface velocity w_s for $Ma = 10,400$ at $t = 10.5$ s.

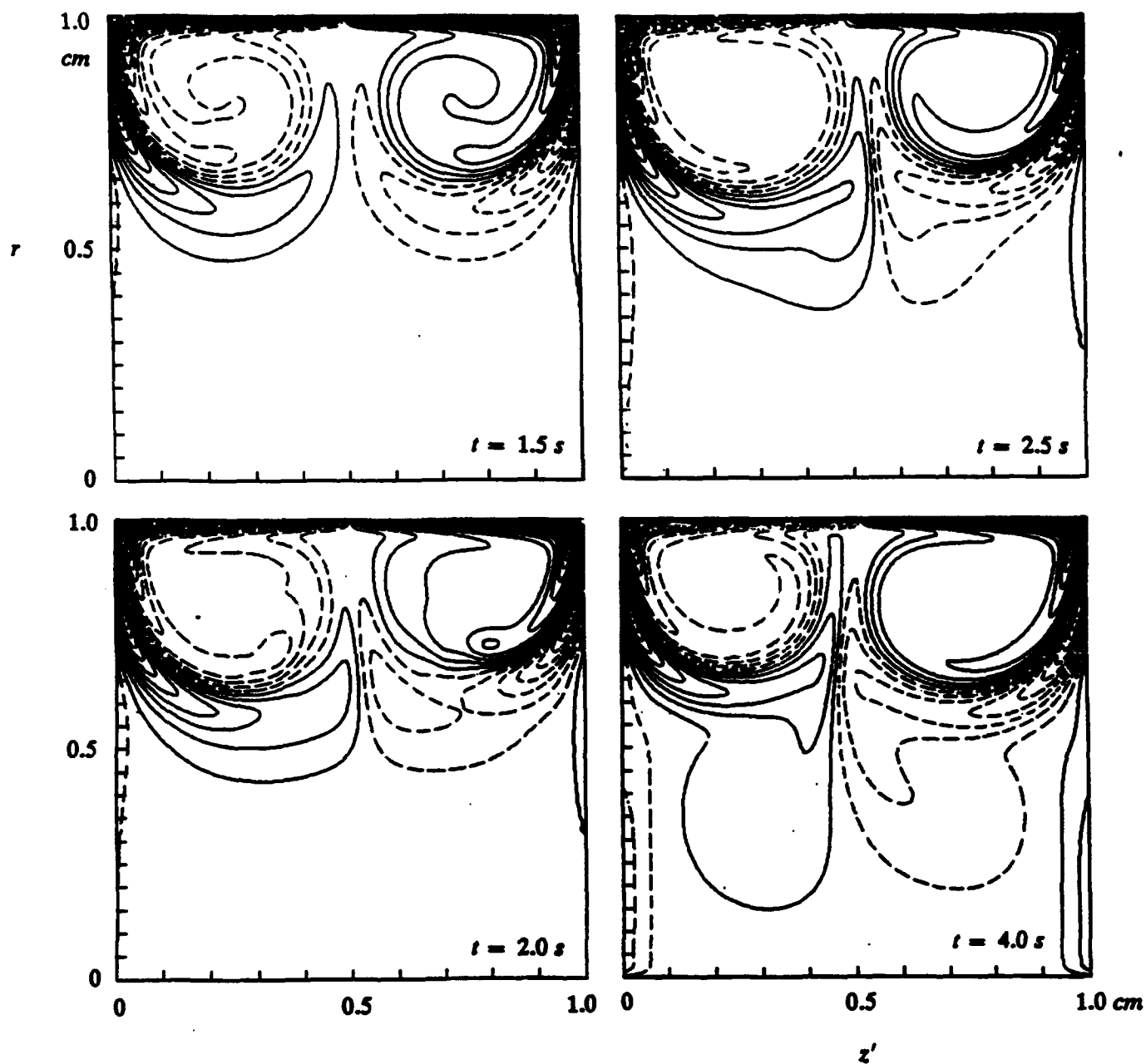


Fig. 13. Lines of constant ω_ϕ/r for $Ma = 50,050$ at four different times before and after the asymmetric disturbance. The ω_ϕ/r -contours are ..., -18, -6, +6, +18,

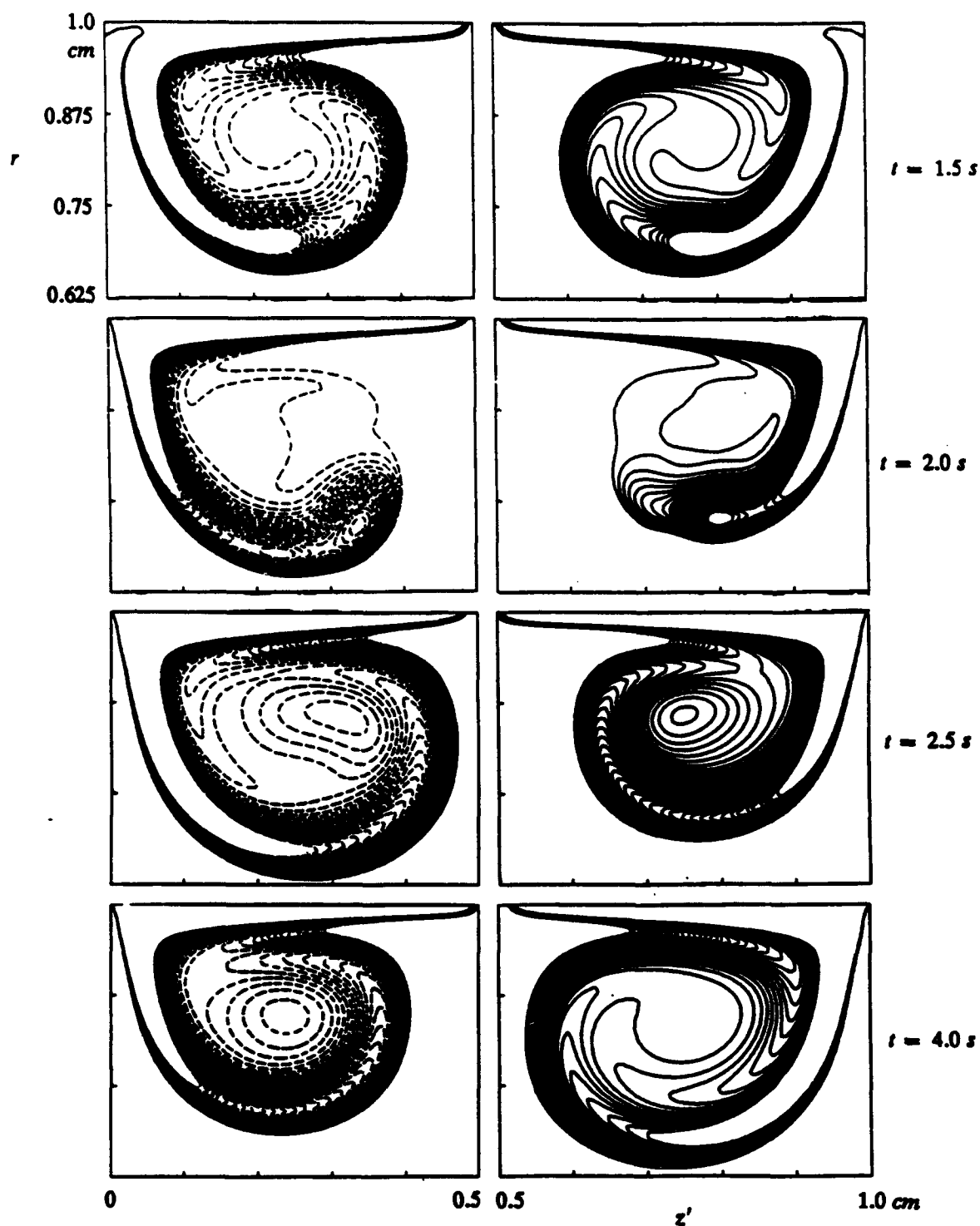


Fig. 14. Lines of constant ω_p/r in the core regions of Fig. 13. The difference in the contour lines is unity for $t = 1.5$ s and 2.0 s, and 0.5 for $t = 2.5$ s and 4.0 s.

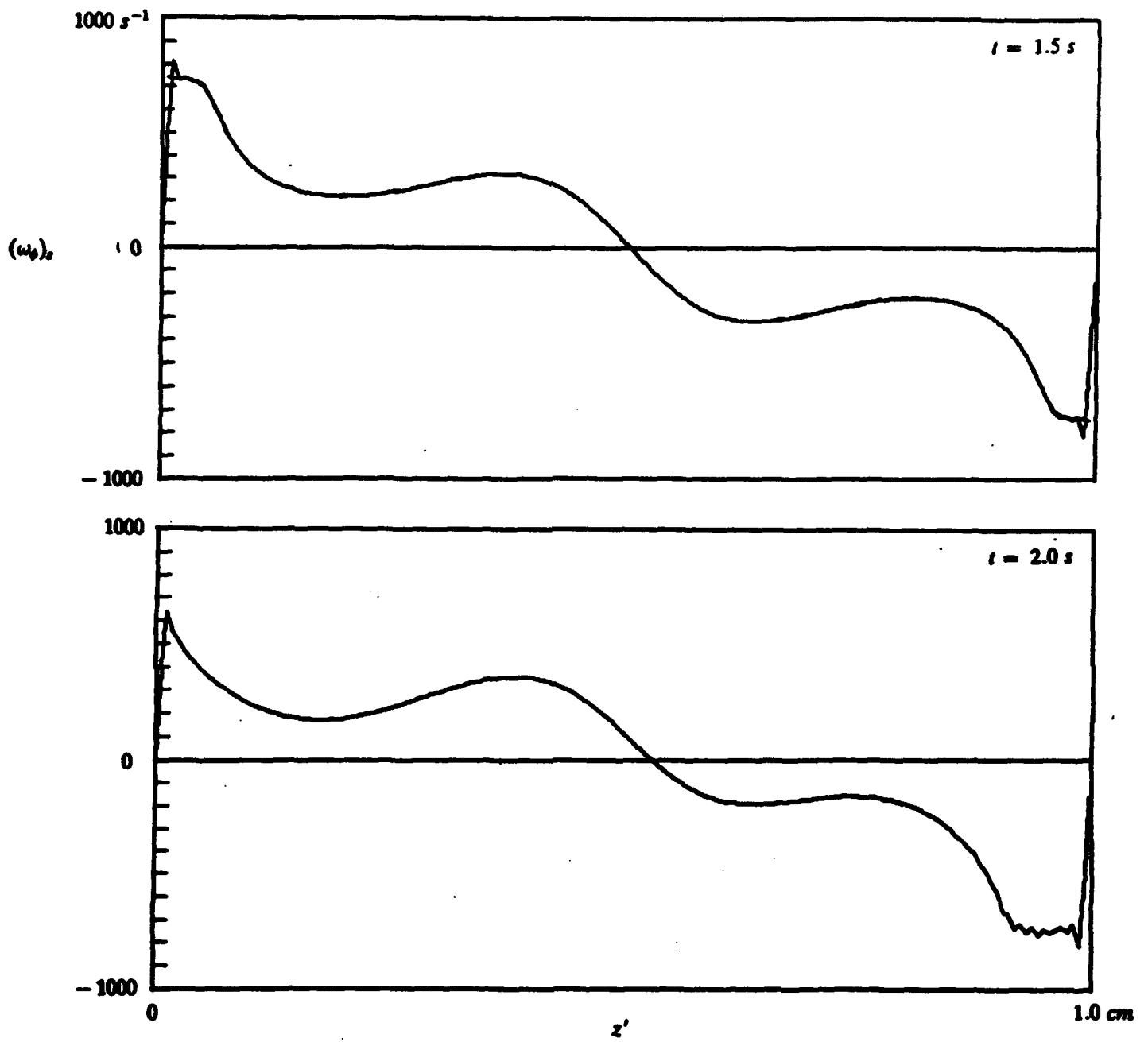


Fig. 15. Surface vorticity for $Ma = 50,050$ of the vorticity field in Fig. 13.

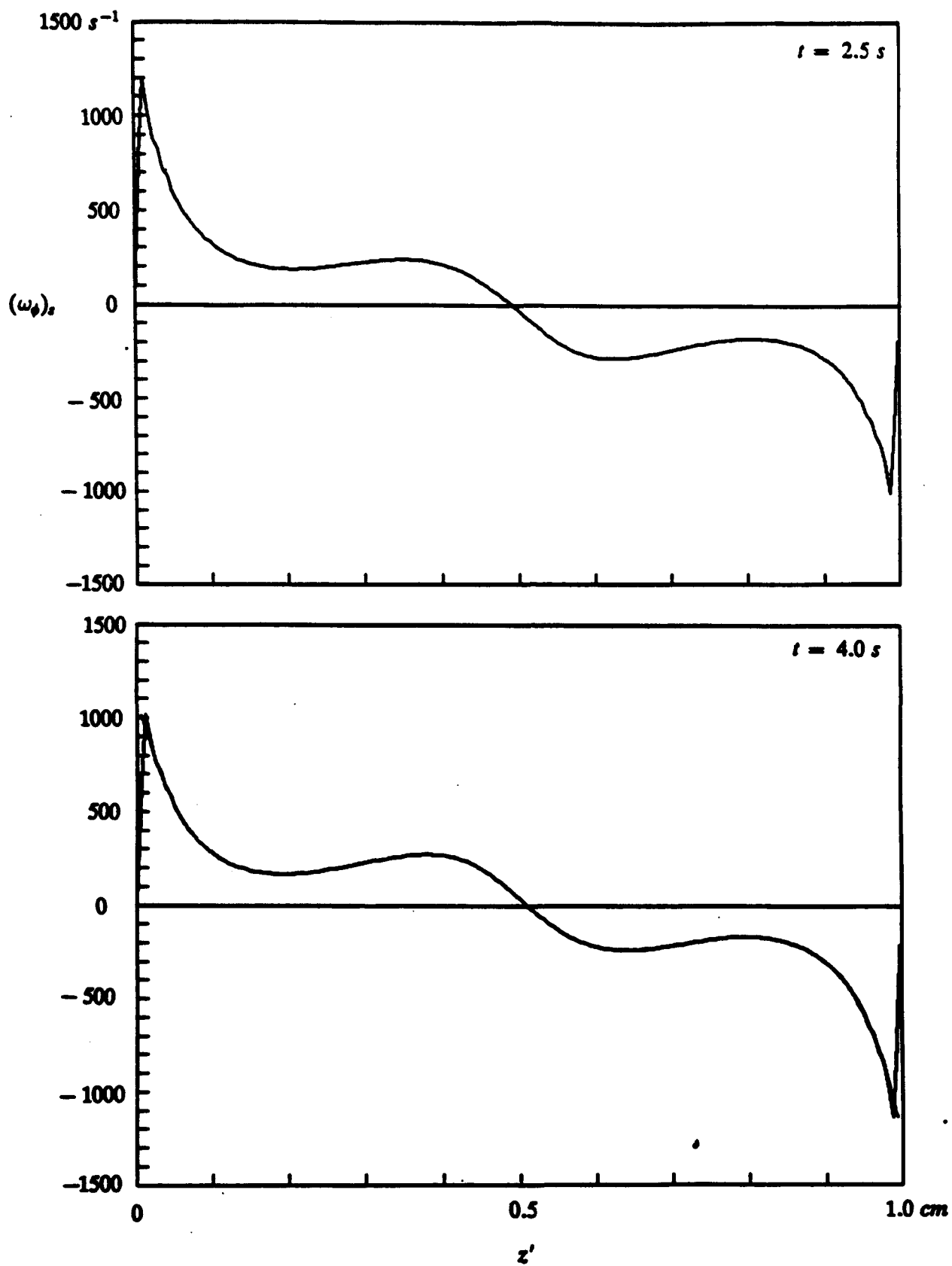


Fig. 15, cont.

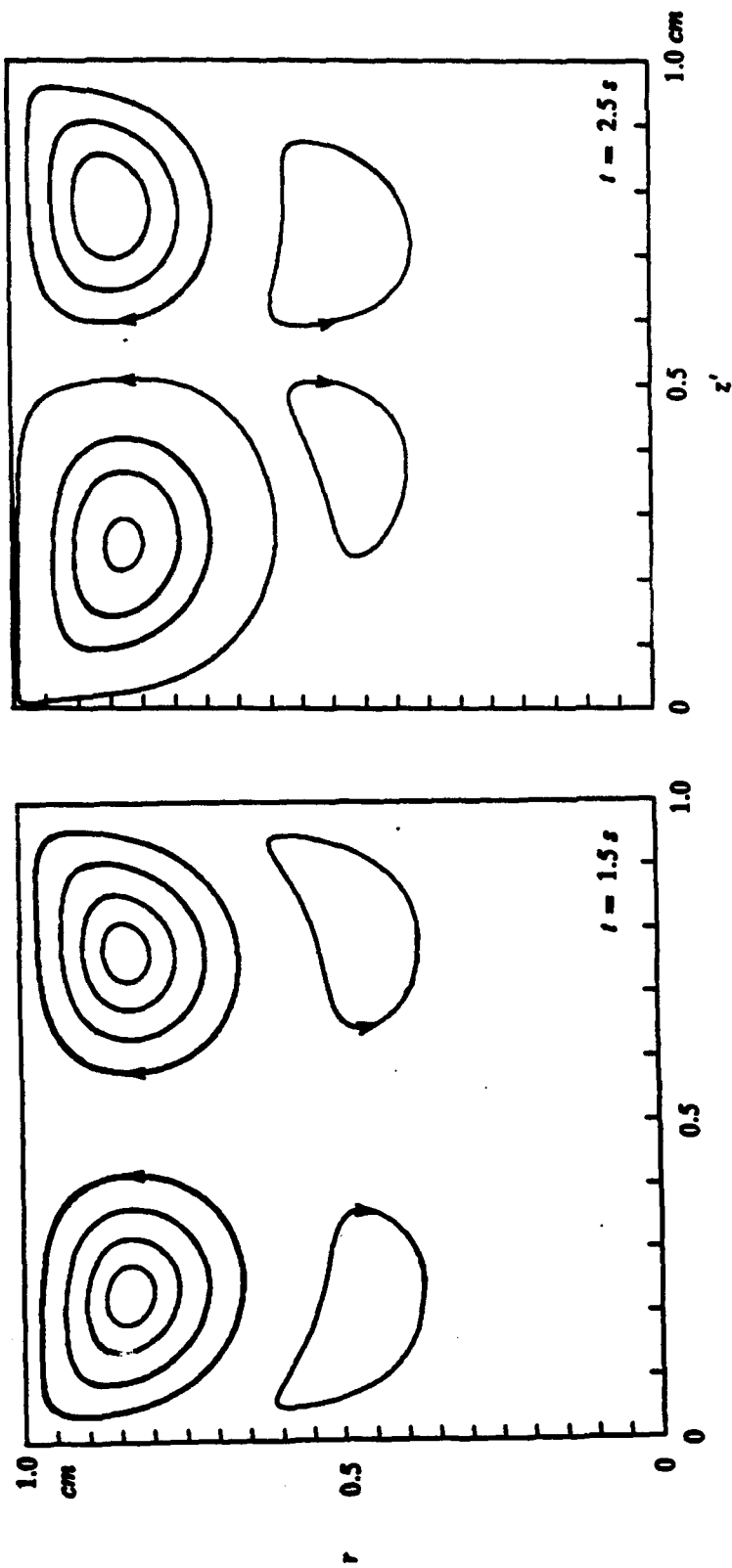


Fig. 16. Streamlines for $Ma = 50,050$ at two different times.

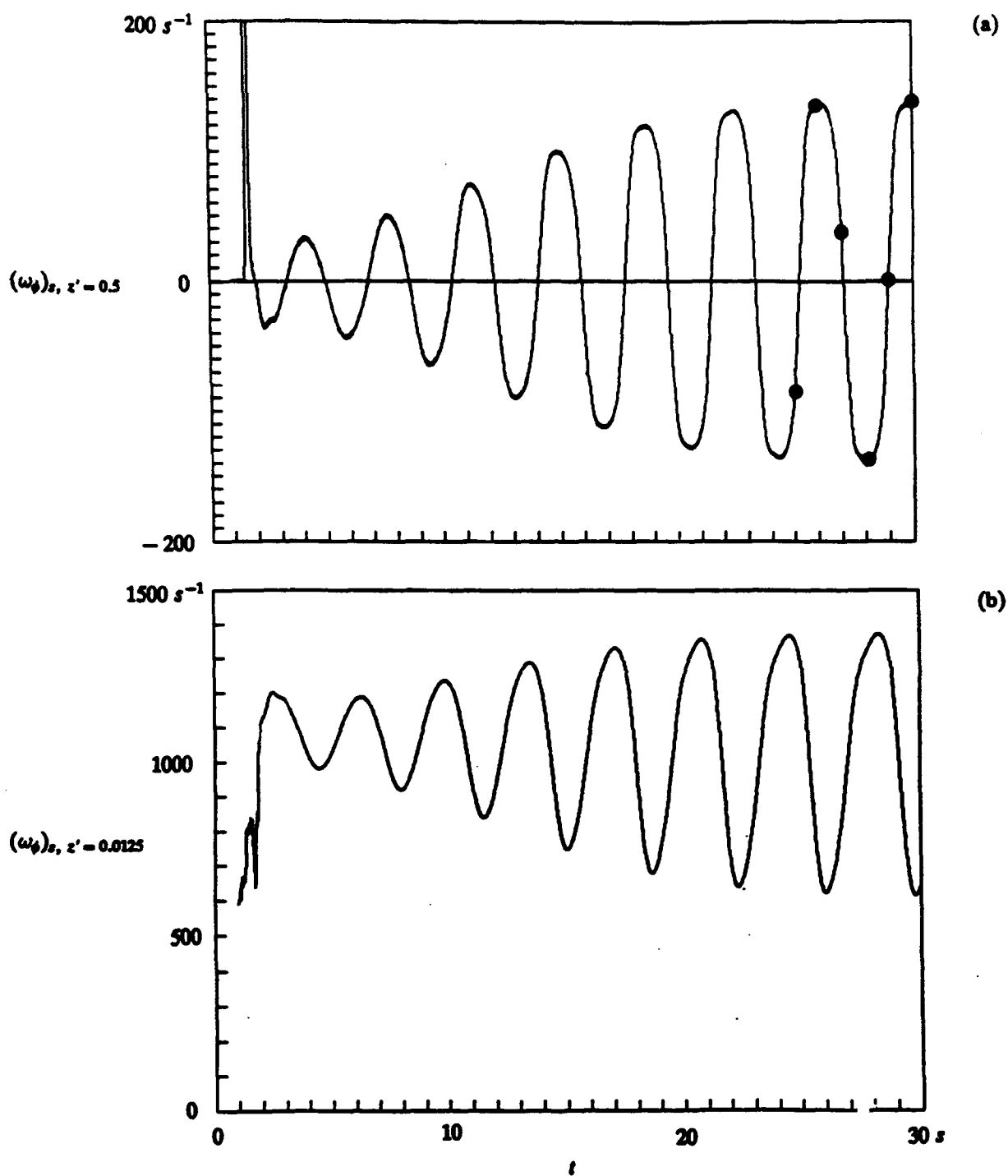


Fig. 17. Surface vorticity for $Ma = 50,050$ (a) at $z' = 0.5$ cm and (b) at $z' = 0.0125$ cm as a function of time. The dots indicate instants which have been selected for studying a cycle.

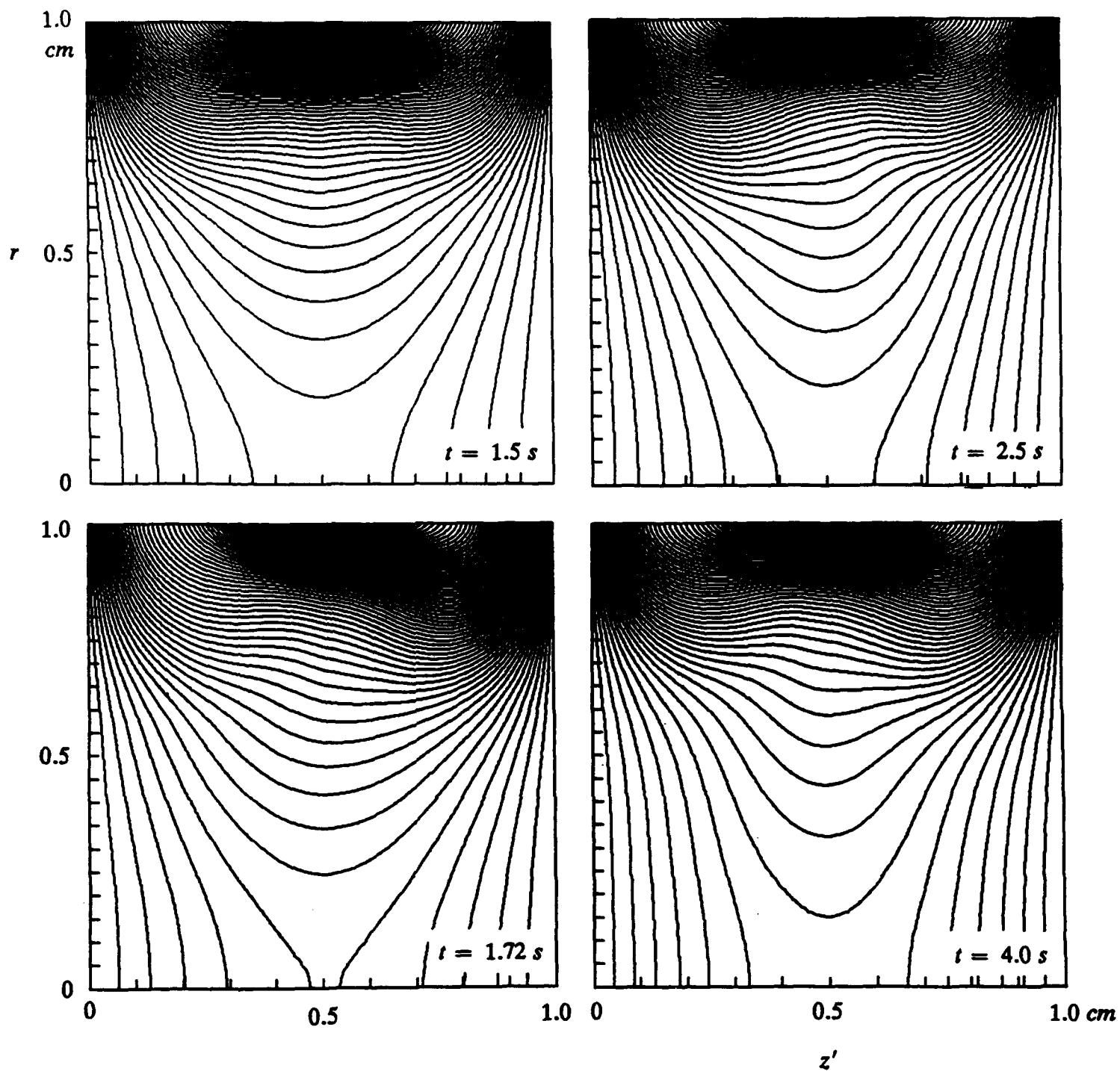


Fig. 18. Isotherms for $Ma = 50,050$ at the times $t = 1.5, 1.72, 2.5, 4.0\text{ s}$. The $T - T_M$ - contours are 0.04, 0.08, ..., 3.28.

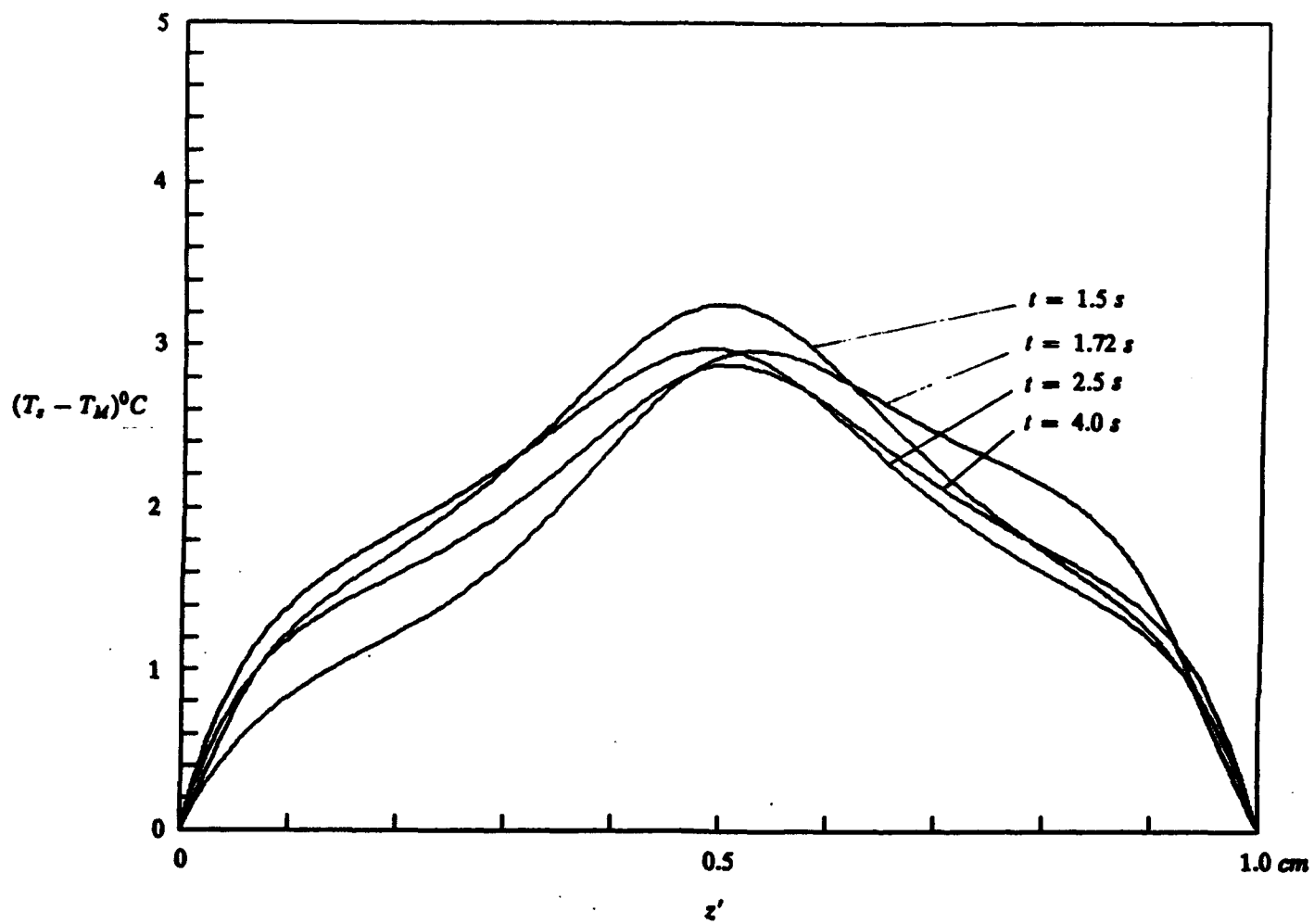


Fig. 19. Surface temperature for $Ma = 50,050$ of the temperature field in Fig. 18.

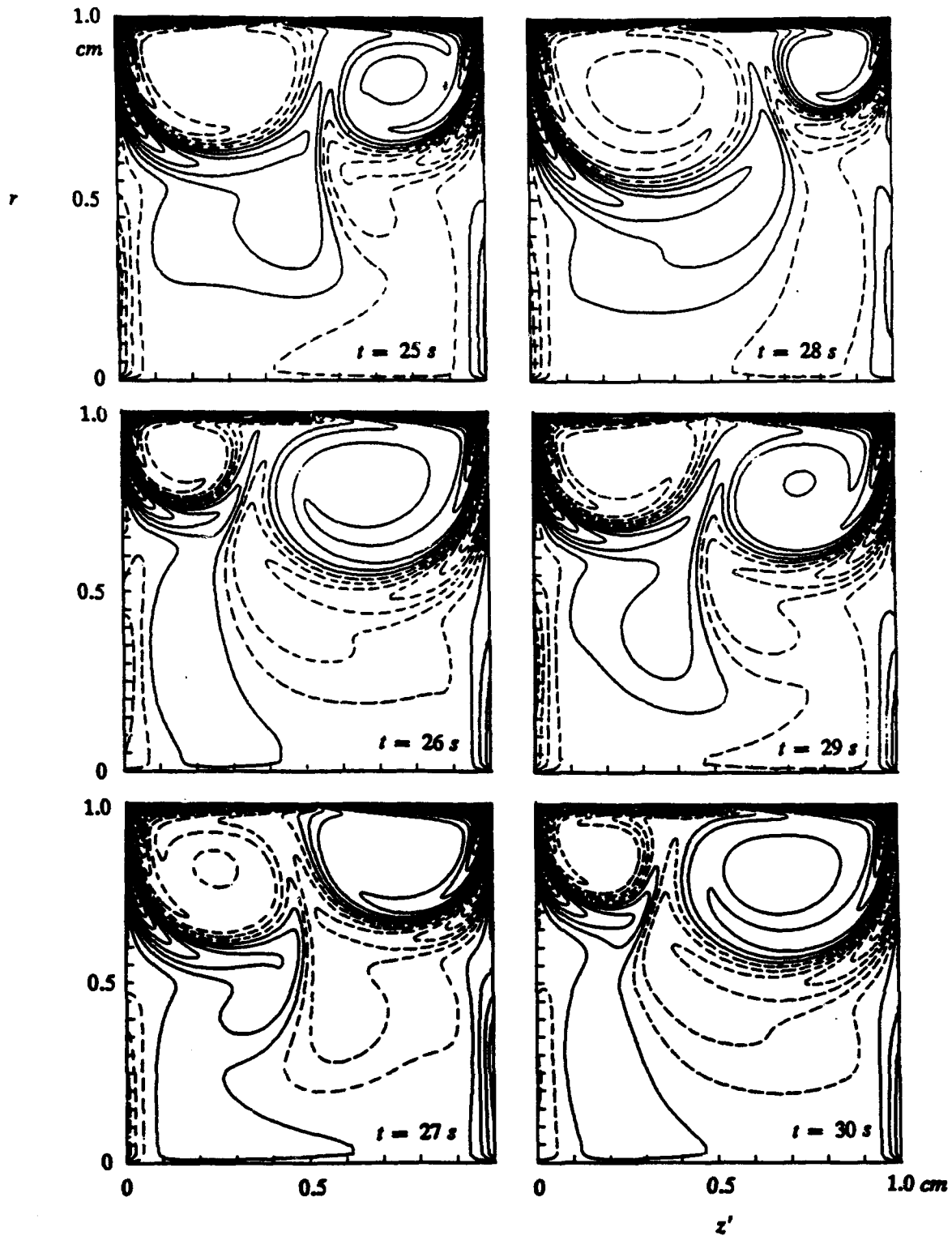


Fig. 20. Lines of constant ω_ϕ/r of a $5/4$ cycle computed for $Ma = 50,050$ at six different times. The ω_ϕ/r - contours are $\dots, -18, -6, +6, +18, \dots$

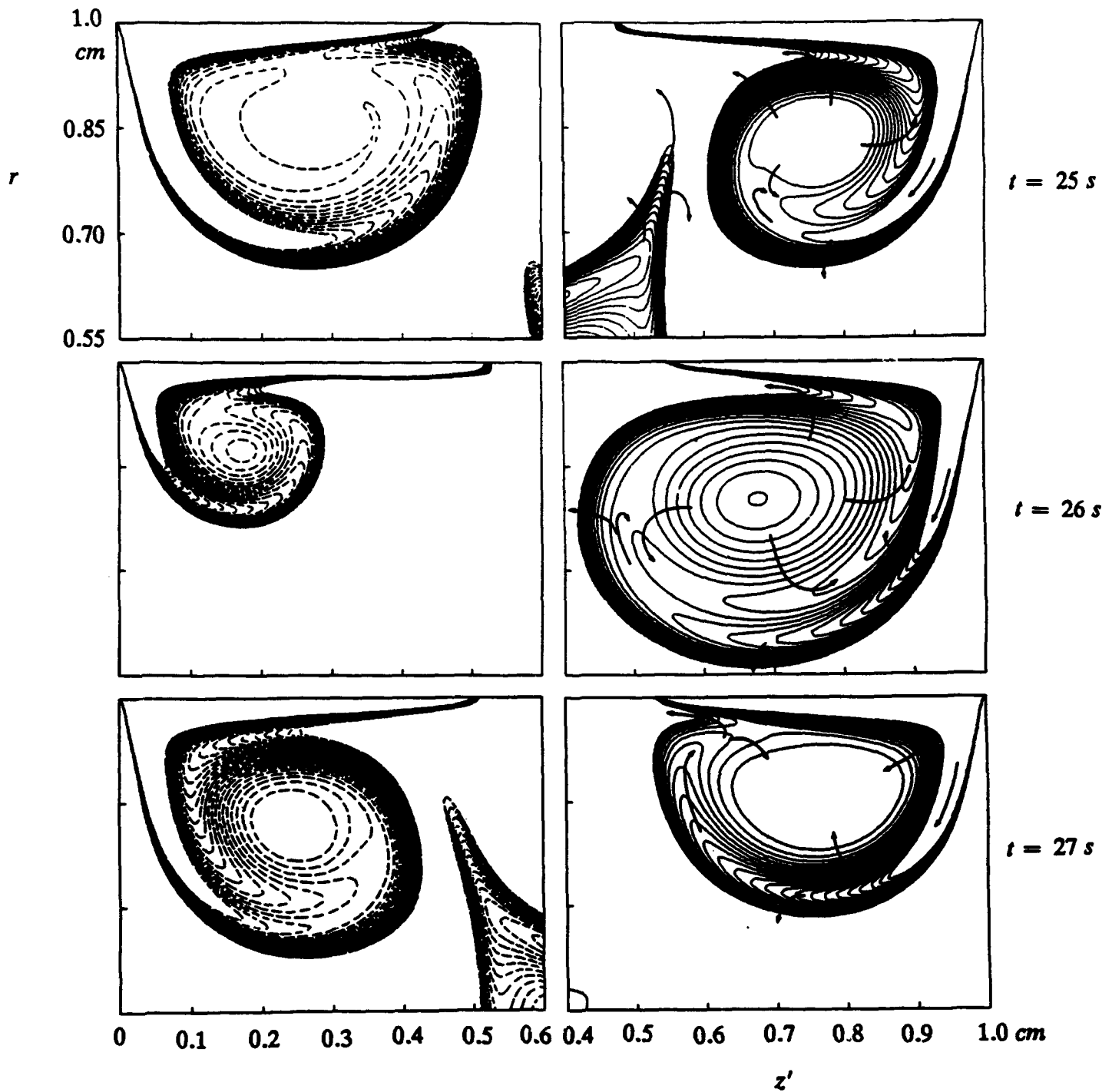


Fig. 21. Lines of constant ω_ϕ/r in the core region of the rolls depicted in Fig. 20. The difference in the contour lines is unity.

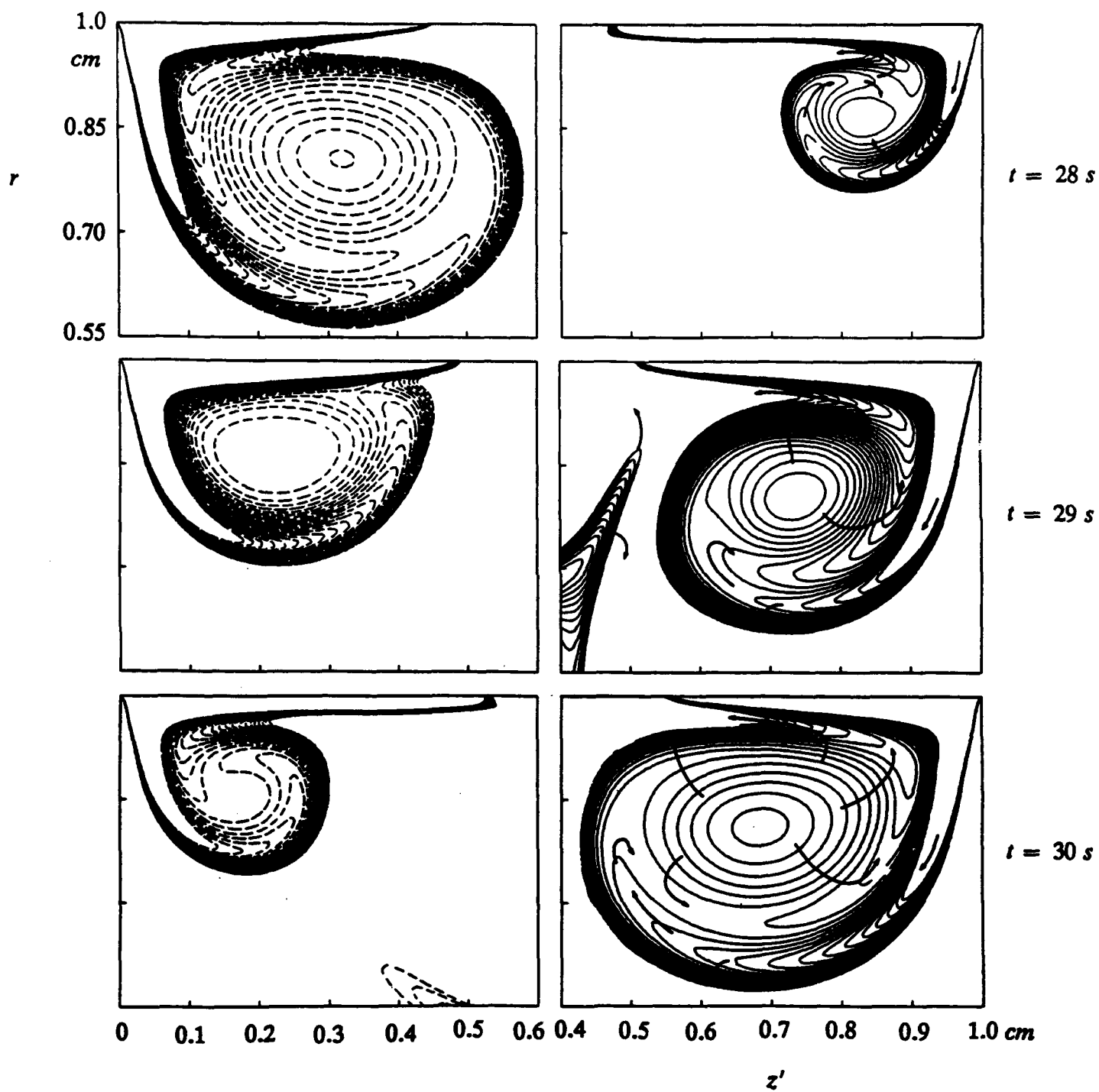


Fig. 21, cont.

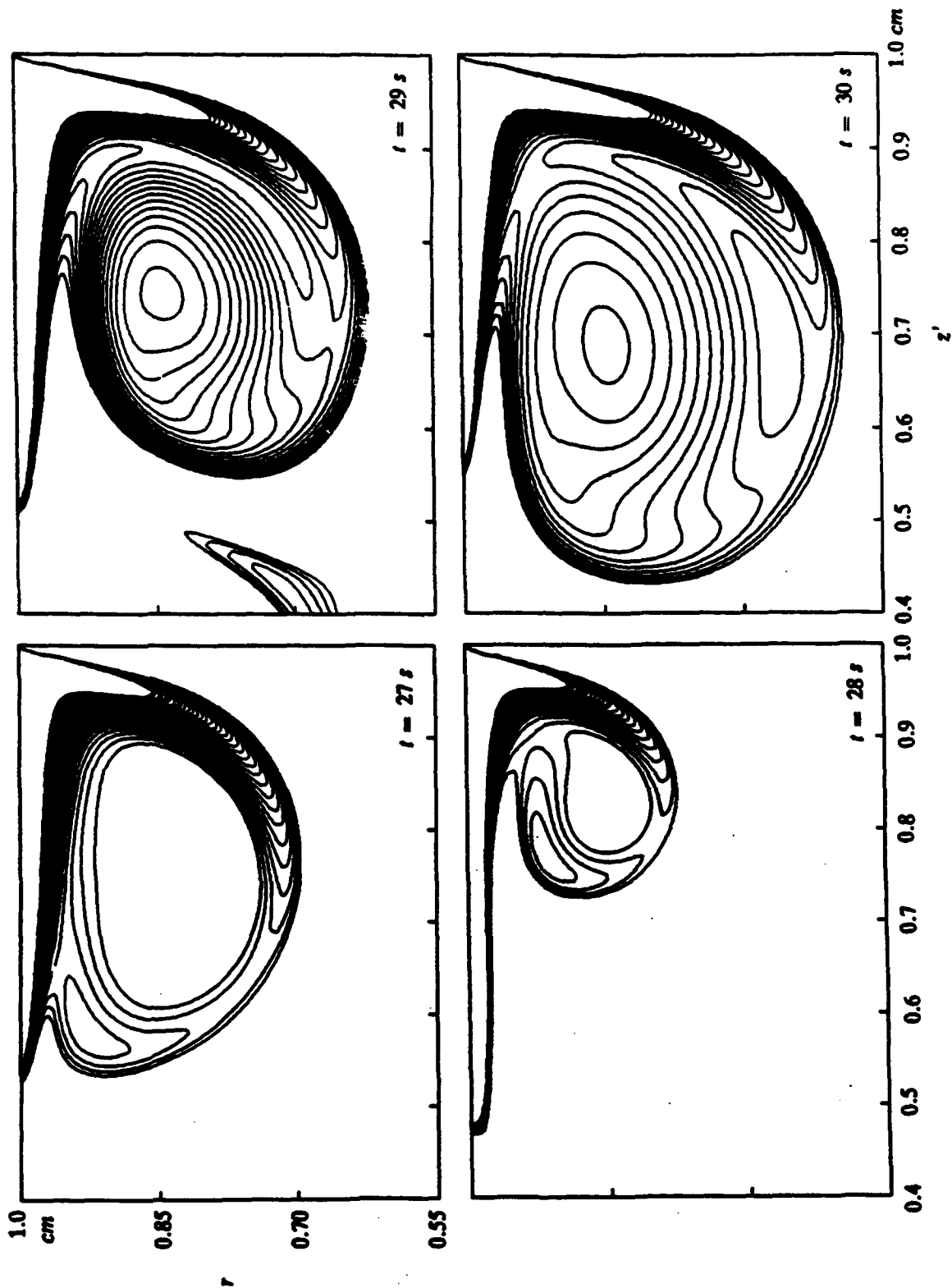


Fig. 22. Equivorticity lines for $Ma = 50,050$ in the right core region at $t = 27, 28, 29, 30\text{ s}$.
The difference in the contour lines is unity.

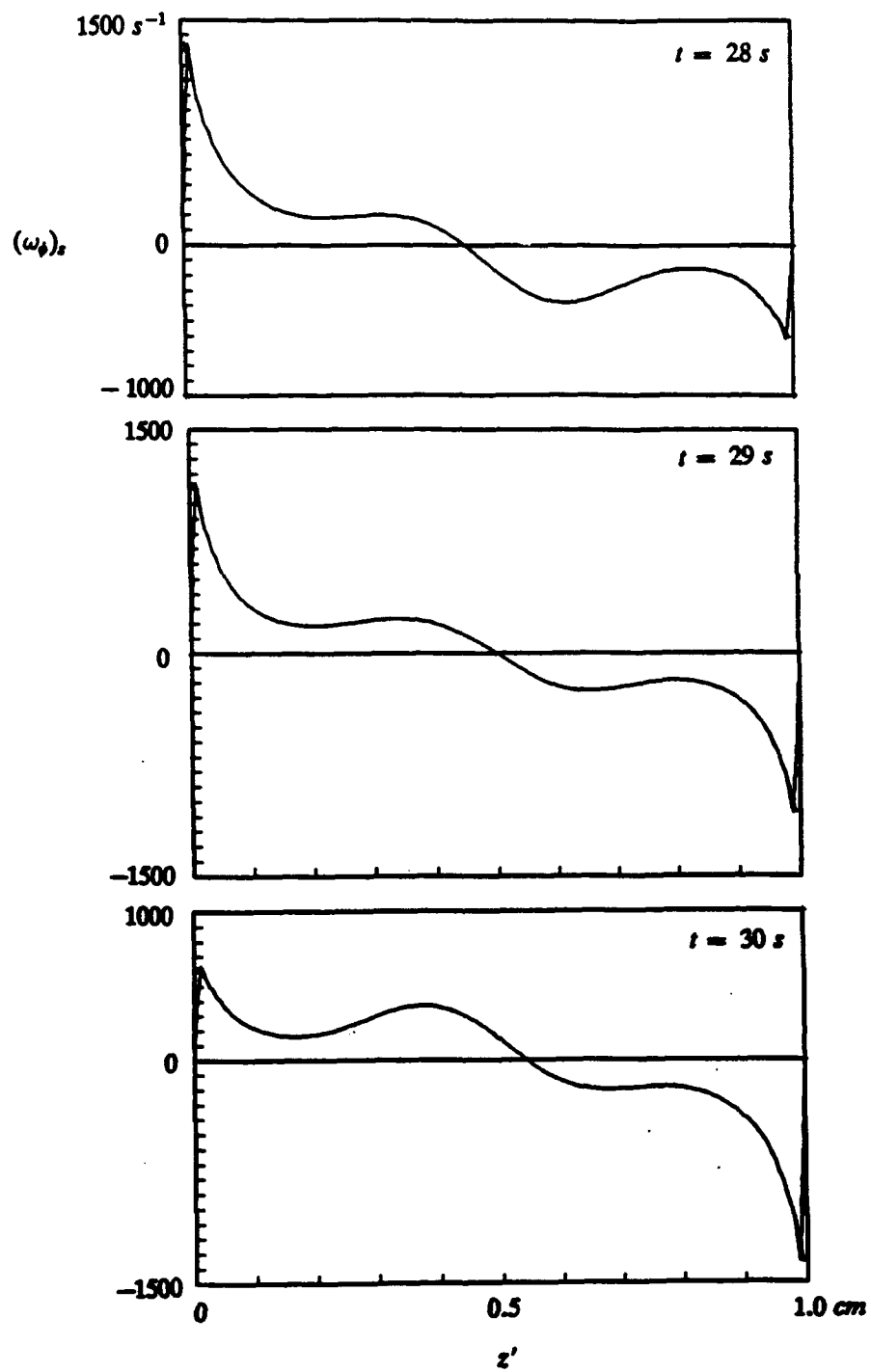


Fig. 23. Surface vorticity for $Ma = 50,050$ of the vorticity field in Fig. 20 at three different times.

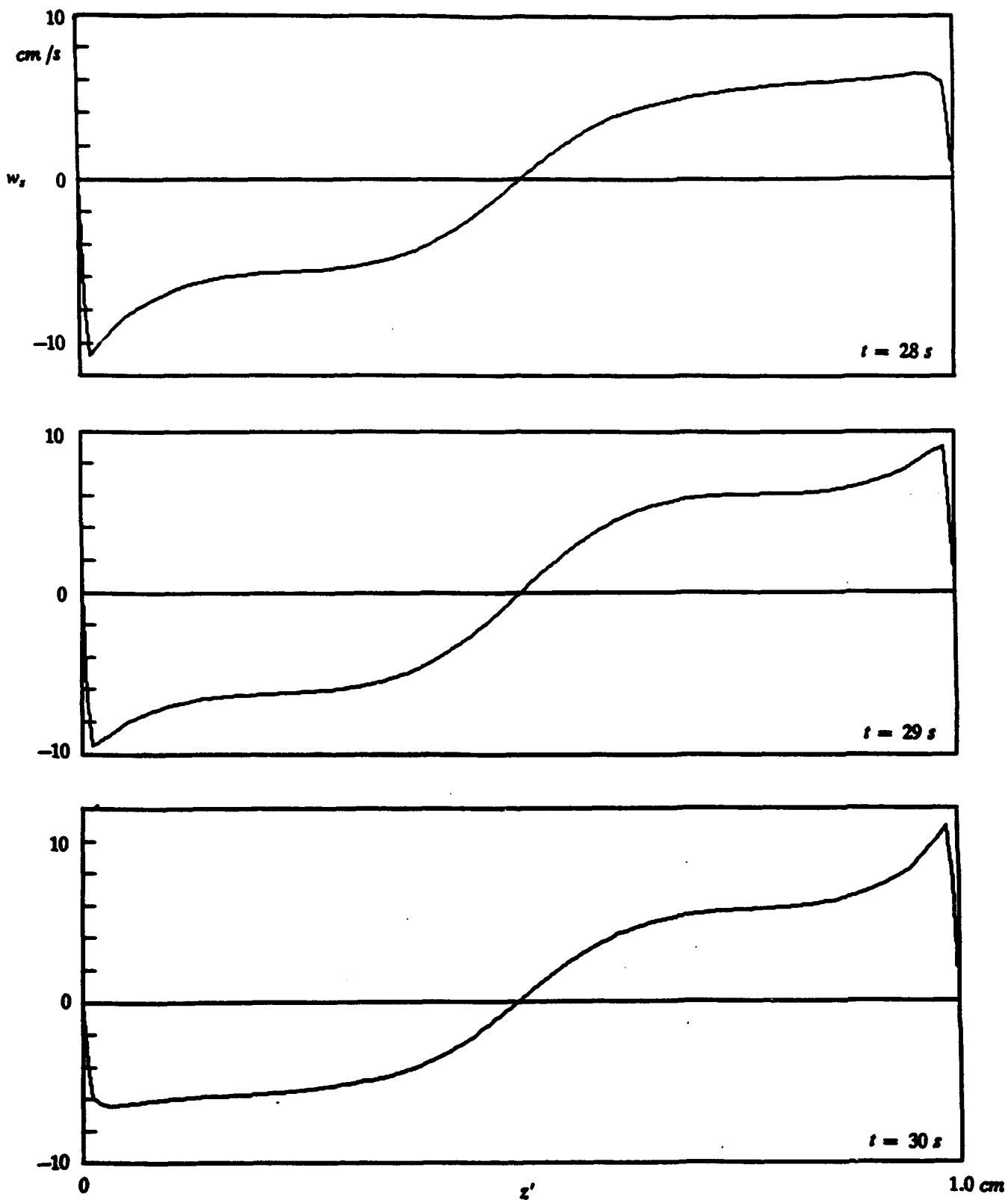


Fig. 24. Surface velocity for $Ma = 50,050$ of the vorticity field in Fig. 20 at three different times.

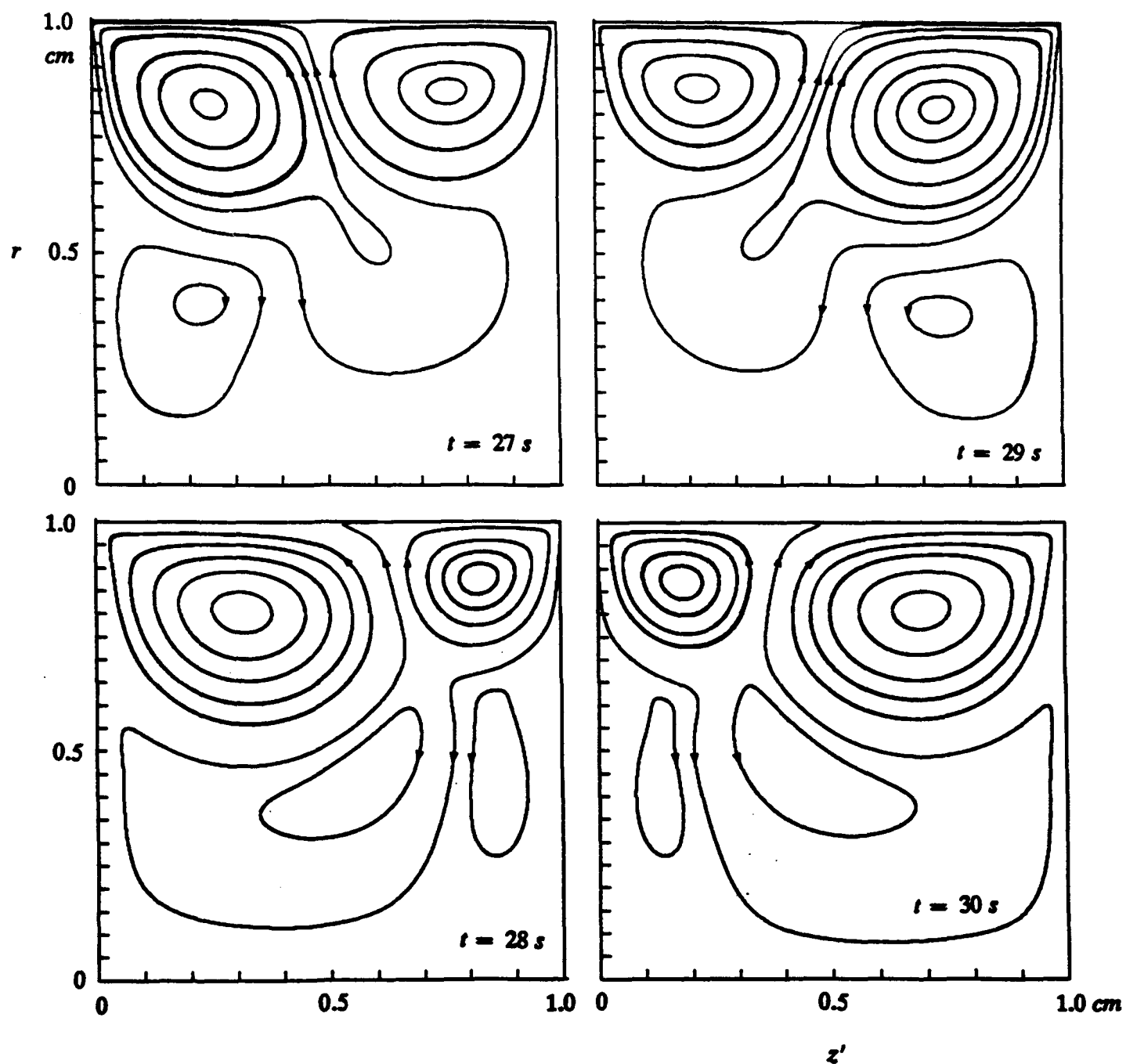


Fig. 25. Streamlines for $Ma = 50,050$ of the vorticity field in Fig. 20 at four different times.

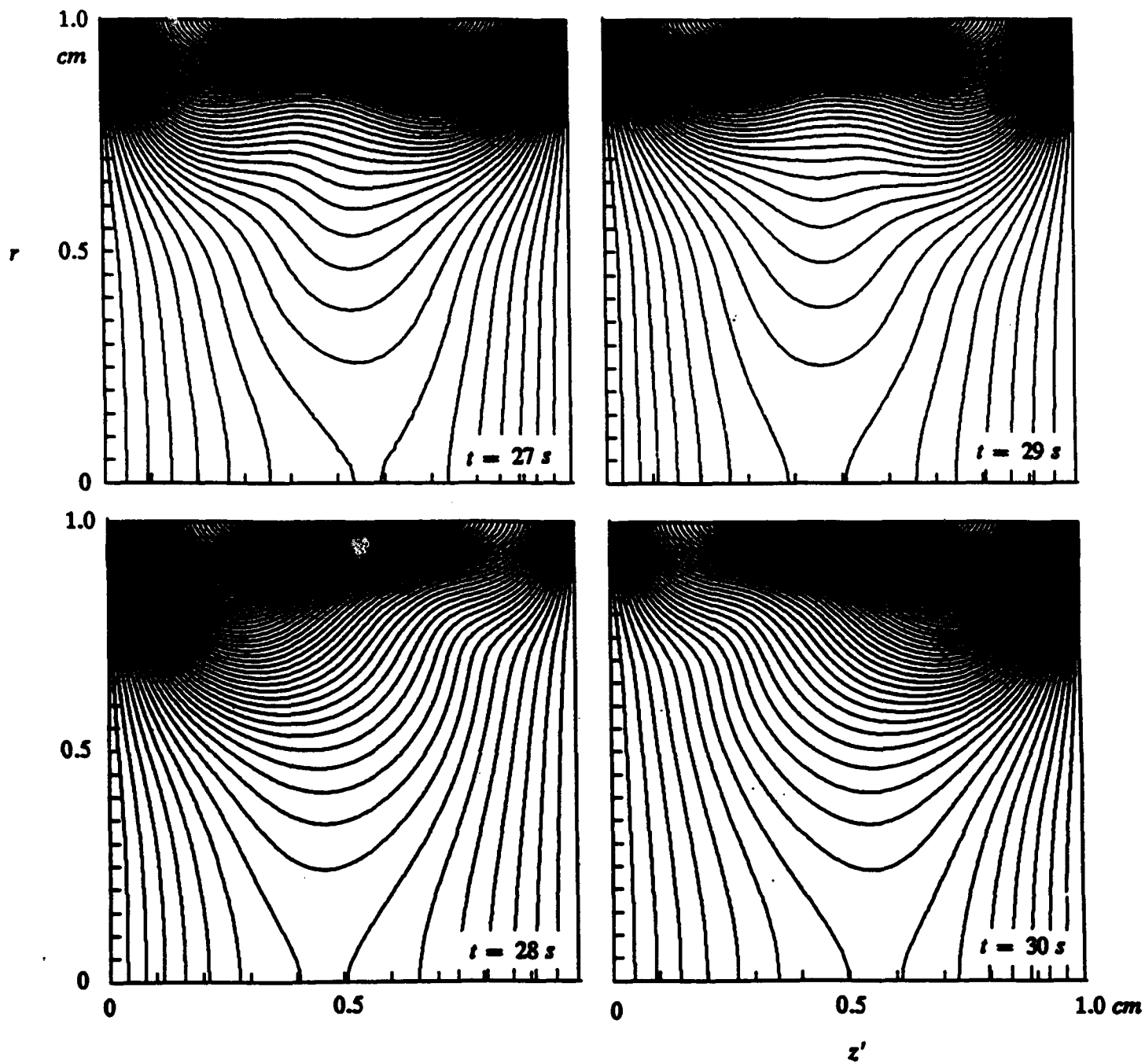


Fig. 26. Isotherms for $Ma = 50,050$ corresponding to the flow field in Fig. 25. The $T - T_M$ - contours are 0.04, 0.08, ..., 3.00.

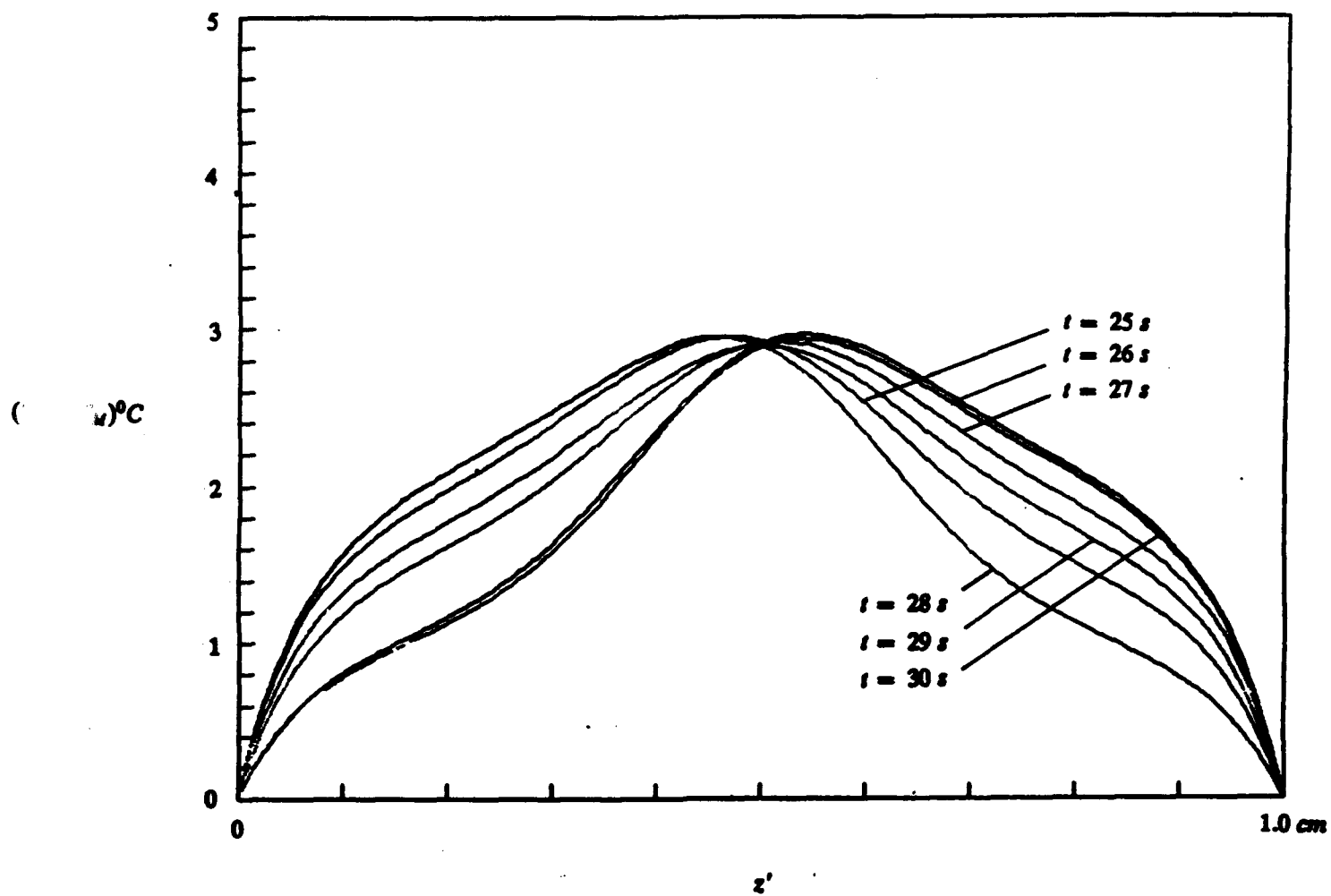


Fig. 27. Surface temperature for $Ma = 50,050$ at six different times in a computed cycle.

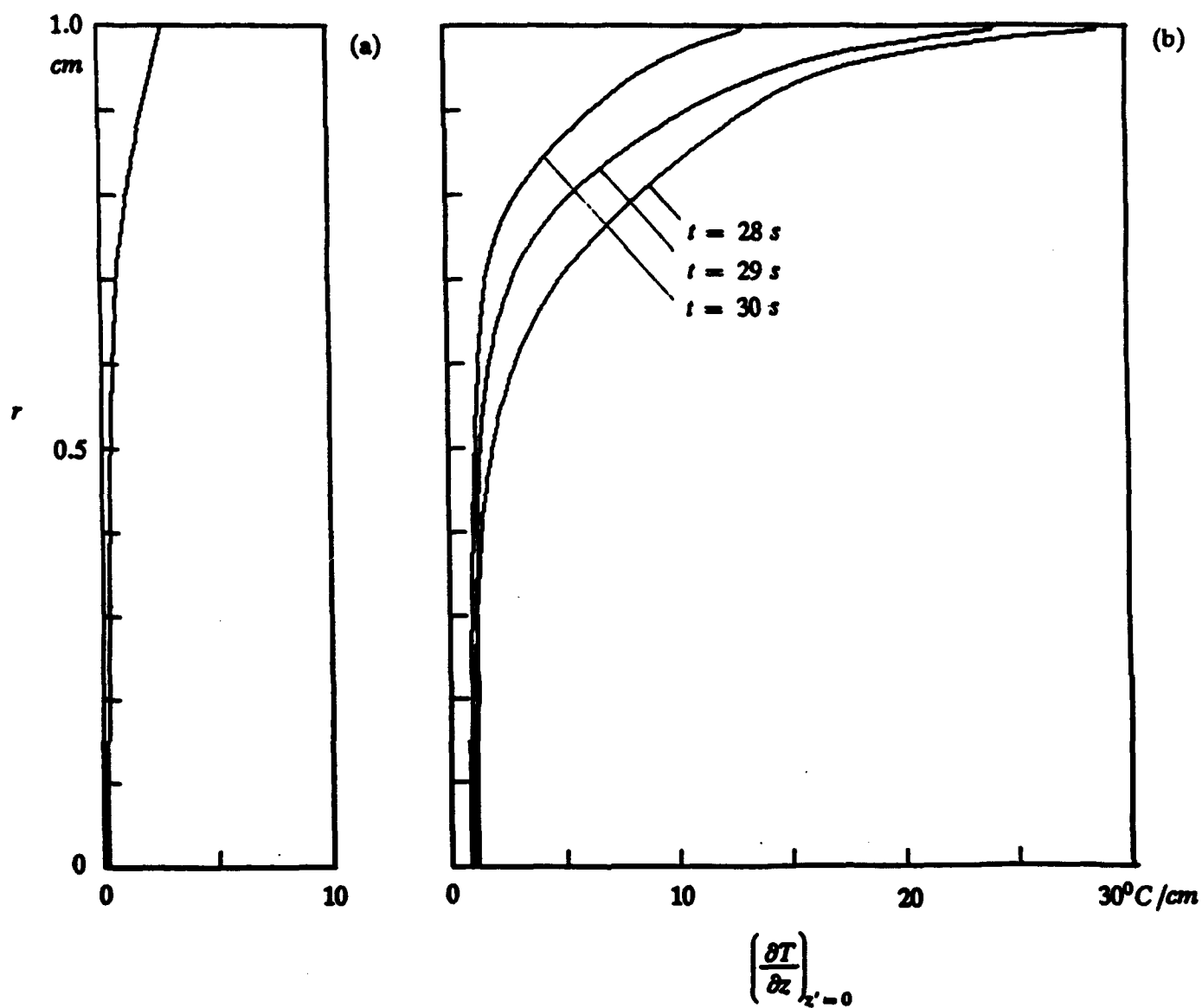


Fig. 28. $\partial T/\partial z$ along the left wall as a measure for the heat flux into the wall. (a) $Ma = 10,400$ at $t = 10.5$ s and (b) $Ma = 50,050$ at $t = 28, 29, 30$ s.

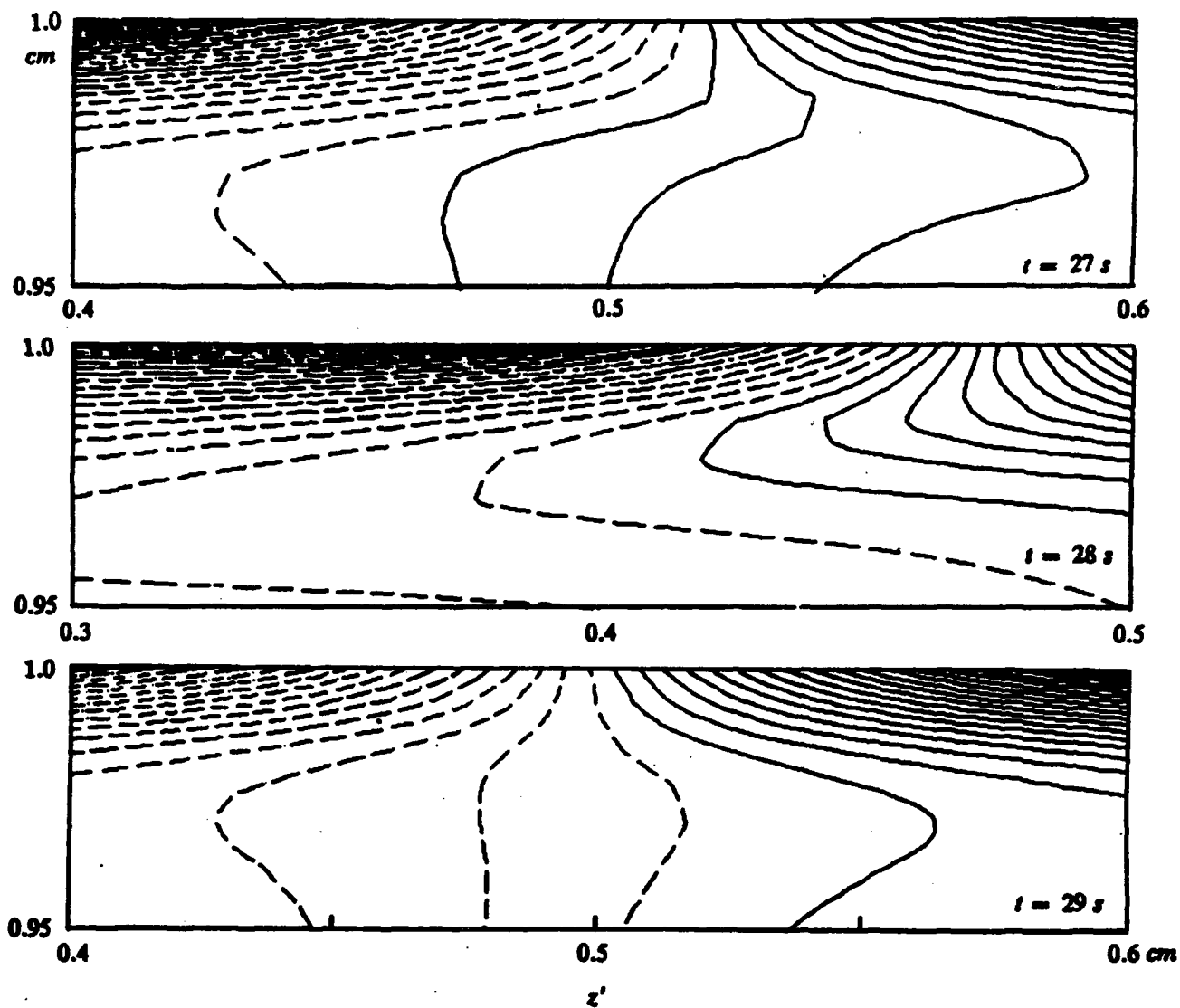
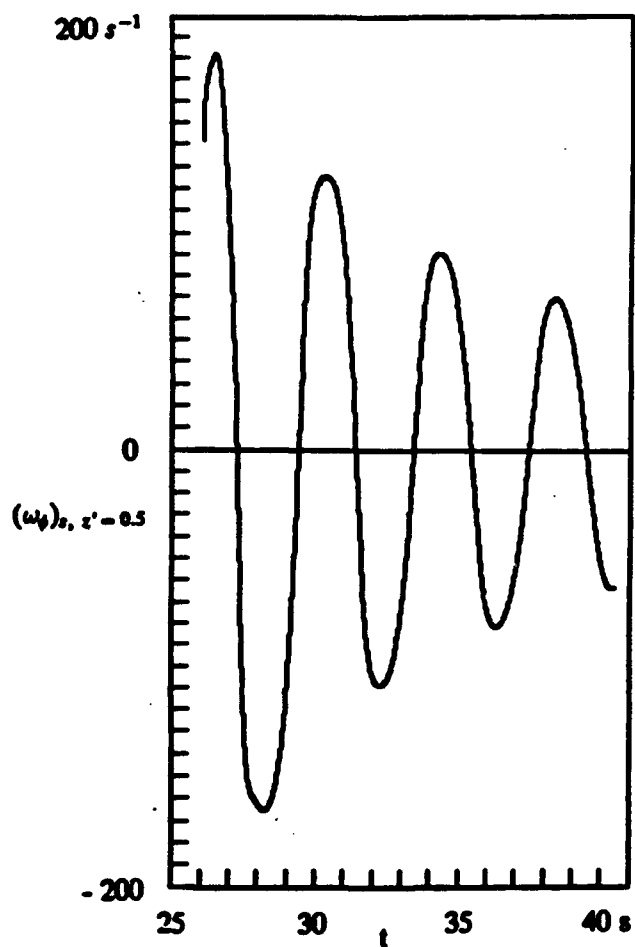
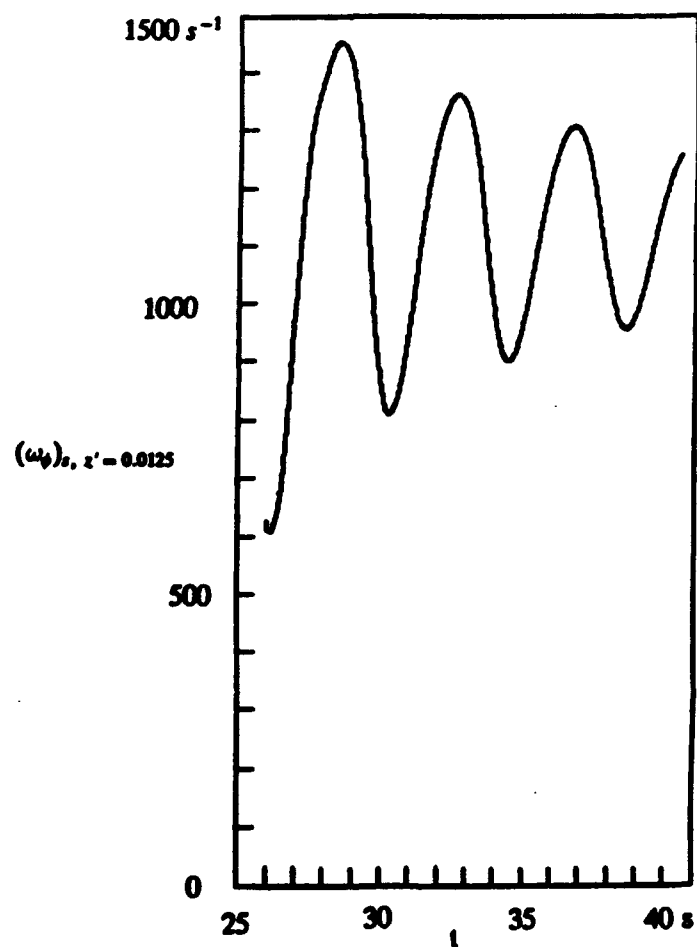


Fig. 29. Close-up of lines of constant ω_ϕ/r for $Ma = 50,050$ near the surface location of $(\omega_\phi)_s = 0$ at $t = 27, 28, 29$ s. The contours are $\dots, -18, -6, +6, +18, \dots$



(a)



(b)

Fig. 30. Surface vorticity on a flat-free surface for $Ma = 50,050$ (a) at $z' = 0.5$ cm and (b) at $z' = 0.0125$ cm as a function of time after the change in the surface conditions at $t = 26$ s.

INITIAL DISTRIBUTION

Copies	Code	Name
--------	------	------

1	ARPA	
3	ONR	
1		J. Fein
1		M. Reischmann
1		E.P. Rood

1	NAVSEA/Lib	
---	------------	--

1	USNA/Tech Lib	
---	---------------	--

1	NRL/Lib	
---	---------	--

2	NAVPGSCOL	
1		Lib
1		T. Sarpkaya

1	NSWC/Dahlgren/Lib	
---	-------------------	--

1	NSWC/Whiteoak/Lib	
---	-------------------	--

2	DTIC	
---	------	--

1	Library of Congress	
1		Science and Tech Division

2	NASA HQ Washington, DC	
1		B. Carpenter
1		Lib

1	NASA Langley Res. Center/Lib	
---	------------------------------	--

1	NASA Ames Res. Center/Lib	
---	---------------------------	--

3	NASA Lewis Res. Center/Lib	
1		J. Salzman
1		J.C. Duh
1		Lib

1	Air Force Flight Dynamics	
		Lab/Lib

1	U.S. Army Res Lab,	
		Aberdeen/Lib

1	NIST/Lib	
---	----------	--

1	Univ of California, Berkeley/Lib	
---	----------------------------------	--

1	Univ of California, San Diego/Lib	
---	-----------------------------------	--

1	Calif Inst of Tech/Lib	
---	------------------------	--

1	Lawrence Livermore Nat	
		Lab /Lib

1	Univ of Maryland /Lib	
---	-----------------------	--

1	Univ of Michigan/Lib	
---	----------------------	--

1	MIT/Lib	
---	---------	--

CENTER DISTRIBUTION

Copies	Code	Name
--------	------	------

1	00	D. Kruse
1	01	R. Metry
1	011	J.A. Corrado
1	0112	B. Douglas
1	0117	B. Nakonechny

1	20	H. Chaplin
1	204	M. Hurwitz
20	2040.1	H.J. Lugt
1	2041	R.T. Van Eseltine
20	2041	S. Ohring

1	3421	TIC (C)
1	3422	TIC (A)
6	3432	Reports Control

1	50	W.B. Morgan
---	----	-------------

1	60	G. Wacker
1	615	R. DeNale
1	615	M. Vassilaros